VISIBLE SPECTRAL REFLECTANCE MEASUREMENTS OF THE GALILEAN SATELLITES OF JUPITER (MORE)

by

LUCY-ANN A. MCFADDEN

B.A. Hampshire College, 1974

SUBMITTED IN PARTIAL FULFILLMENT OF

THE REQUIREMENTS FOR THE

DEGREE OF

MASTER OF SCIENCE

at the

MASSACHUSETTS INSTITUTE OF TECHNOLOGY

February, 1977

Signature of Author.....
Department of Earth & Planetary Science, January 21, 1977

Certified by.....
Thesis Supervisor

Accepted by .....
Chairman, Departmental Committee on Graduate Students,
Earth & Planetary Sciences

1 Lindgren
WITHDRAWN
MAR 22 1977
MIT LIBRARIES

VISIBLE SPECTRAL REFLECTANCE MEASUREMENTS OF THE GALILEAN SATELLITES OF JUPITER (MORE)

by

LUCY-ANN A. MCFADDEN

Submitted to the Department of Earth and Planetary Sciences on January 21, 1977 in partial fulfillment of the requirements for the degree of Master of Science.

ABSTRACT

New spectral reflectance measurements of the Galilean satellites of Jupiter were obtained in November, 1975 at the 224 cm. telescope at Mauna Kea Observatory, Hawaii. A prism spectrograph with a silicon vidicon detector was used in the spectral region 0.3-1.06 μm. These new measurements are of a higher wavelength resolution than previous measurements. The results are compared with earlier measurements. In order to make an accurate comparison of the data, the results of Johnson (1970) were re-reduced. Satellite/satellite relative reflectances are also presented and discussed. The measurements presented here were made at one orbital phase. Future observing programs should include broader rotational phase coverage and should extend into the near infrared region of the spectrum. The new and old measurements show sufficient discrepancies to warrant more visible observations.

ACKNOWLEDGEMENTS

I would like to thank Dr. Thomas B. McCord for suggesting this thesis topic and his subsequent supervision of the work I have done. The following people affected the outcome of this project and I would like to thank them: Sol Giles for building the spectrometer, Jeff Bosel for design and maintenance of the vidicon system, Tom McCord and Carle Pieters for making the observations at the telescope, George Fawcett for writing some of the data handling programs, Mike Gaffey and Bob Huguenin for their encouragement and professional advice.

TABLE OF CONTENTS

List of Figures

LIST OF TABLES

Prologue

Io- A maiden loved by Zeus and changed into a heifer by jealous Hera, or in some tails by Zeus, to protect her; she was watched by hundred-eyed Argus and driven to Egypt where she remained in her natural form.

Europa- A Phoenician princess loved by Zeus;taking on the form of a white bull, he carried her off across the sea to Crete.

Ganymede- A beautiful youth carried off by Zeus to be the cupbearer to the gods.

Callisto- A nymph who, because she was loved by Zeus, was changed into a bear by Hera; Zeus placed her among the stars in the constellation the Bear.

INTRODUCTION

The first photometric observations of the Galilean satellites of Jupiter in modern times determined the variation in brightness as a function of rotational and solar phase angle. These measurements, made by Stebbins (1927) and Stebbins & Jacobsen (1928) were reported in a clear, concise and leisurely fashion which is a delight to read today. Their results showed that the leading side of Io is brighter than the trailing side by about 0.21 magnitudes. Io also shows large color variations with orbital phase. The other three satellites are "variable in their period of revolution, and also exhibit a flashing up at full phase" (Stebbins, 1927). The observations reported in the second article show a difference between the solar phase effects on the two sides of Callisto. At opposition Callisto brightens up much more on the front side, the difference being over a tenth of a magnitude. Ganymede is brighter on the trailing side by .002 magnitudes, Io and Europa brighten on the leading side by .037 and .004 magnitudes respectively.

Harris (1961) reduced Stebbins' and Jacobsen's measurements to the standard UBV system of Johnson and Morgan (1953). Additional observations of the Galilean satellites were made at McDonald Observatory between 1950 and 1954 to check the earlier measurements, and confirmed the conclusions of Stebbins and Jacobsen. Color diferences were reported for the first time and it was remarked that the variations in color with orbital phase for Io is quite large ("outstanding"). For Europa, the trailing side was found to be 20% fainter in the ultraviolet (UV) than the leading side. A light variation in U-B color

is observed for Ganymede. Negligible variation in both B-V and U-B was observed for Callisto. The large increase in brightness at opposition was confirmed and attributed to the absence of shadows normally present, except at opposition, due to surface features.

It appears that the next serious and comprehensive photometric study of these satellites was performed by T. V. Johnson (1969). Reasonable rotational and solar phase angle coverage (0-9°) was added to earlier measurements. Again no striking discoveries were made in terms of the solar phase and orbital brightness and color characteristics.

Subsequent three and four color photometric studies of the Galilean satellites have been done by Morrison et. al. (1974), Blanco & Catalano (1974) and Millis & Thompson (1975). They have all tried to present more precise, well calibrated magnitudes and colors, and parameters defining the solar phase effect (necessary for mutual occultation data reduction). Valuable additions have been made to the data base, but each study encounters problems in obtaining adequate coverage of solar and rotational phase. Added to this are the problems of finding standard stars in the vicinity of the satellites, eliminating scattered light from Jupiter, developing new ideas on how to separate the rotational from the solar phase effects and presenting these differences. The result is data which is difficult to compare for consistency.

Since the study by Harris (1961) the standard UBV system of Johnson & Morgan (1951, 1953) has been superceded by the ubvy system of Crawford (1966) for planet photometry. However the standard magnitude

is still the V of the UBV, and Millis & Thompson (1975) and Blanco & Catalano (1974) carried out their entire study with UBV filters, which are spectrally wider than the ubvy filters. The goal of Blanco & Catalano was to determine the corresponding maximum and minimum of the rotational light curves. But to do this they had to correct for the solar phase effect, for which they determined phase coefficients. Their results showed that the orbital phase at which minimum brightness occurs shifts westward from J1-J4.

The major contribution of the Morrison et. al. paper is the manner in which they represent the solar phase effect. The three parameters are V at $\alpha = 6^{o}$, $dv/d\alpha$ for $\alpha > 6^{o}$ and V at $\alpha = 0^{o}$ instead of the A and B coefficients used by Stebbins. The new parameters are more readily compared with the photometric parameters of other solar system objects which have a linear phase effect at $\alpha > 7^{o}$ and an opposition surge for $\alpha < 7^{o}$. The discussion by Morrison et. al. contains what amounts to verbal, comparative color maps of the four Galilean satellites. The newer measurements agree with those made by Blanco & Catalano (1974) for Callisto and Ganymede for V magnitude measurements. Io and Europa V magnitudes are larger than previous measurements. Millis & Thompson also noted what appears to be an increase in brightness in their measurements suggesting secular light variations, when they could provide no other explanation.

The first extensive study of the spectral reflectance of the Galilean satellites is by Johnson (1969) and Johnson & McCord(1970). An earlier paper by McNamara (1964) presented reflectance measurements

betweem .3176 μm and .620 μm. The standard visible spectral region which was used by Johnson has come to be .35 - 1.1 μm, a standard defined by detector sensitivity. The spectral refectance of the four Galilean satellites from Johnson & McCord (1970)and Wamsteker (1972) are shown in figure 5-8. A noticable feature is a steep slope in the UV for all four satellites; it is strongest for Io and decreases for each satellite with increasing distance from Jupiter. A weak absorption feature is present between .5 and .6 μm in Io's spectrum. A shallow absorption feature is present at .8 μm for both Io and Callisto's spectrum. The reflectance decreases beyond 1.0 μm for all four satellites. Johnson & McCord (1970) note that the reflectance of the four satellites differ markedly from those of the Moon or Mars.

Other visible observations are difficult to compare with spectral reflectance measurements because the reflectance data is lost in the reduction procedure or the observing program was not intended to determine spectral reflectance but rather to measure rotational effects or albedo variations (Lee, 1971). Even measurements which are comparable do not agree well (figures 5-8).

A precise interpretation of the satellites' visible reflectance curves was not available in 1970, nor is it now. Laboratory investigations have been carried out for just this purpose but have not been totally successful.

Infrared Observations

Infrared measurements have been available since 1957 when Kuiper measured the brightness of the satellites at 1 and 2 μm and showed by dividing the albedos at these two wavelengths, that Io and Callisto

remain practically constant in brightness from 1-2 μm but Europa and Ganymede are deficient in reflection at the longer wavelengths (Harris, 1961, Kuiper, 1973). Low resolution spectra also produced the same results (Kuiper, 1957, 1973). The explanation offered for these results was the one still accepted today; that Europa is covered with water ice and Ganymede may be covered with water ice and contaminated with silicate dust.

Moroz (1966) published data from observations made between 1963 and 1964 in the .7 - 2.5 μm spectral region using a prism spectrometer and a lead sulfide photoresistor. His results agree with those of Kuiper. The paper includes a discussion (no longer up to date because of improved dynamical constants), of the conditions necessary to maintain ice on the satellite surfaces. The theory necessitates the presence of atmospheres on the satellites. However, there is evidence of a tenuous atmosphere only on Io (Kliore et. al., 1974) and Ganymede (Carlson et. al., 1973).

Geometric albedoes were determined from .8 - 2.5 μm (Johnson & McCord 1970) by measurements made with infrared interference filters, a lead sulfide detector and a double beam photometer. The results agree with those of Kuiper (1961) and Moroz (1966). The geometric albedo remains near unity from 1 μm - 2.5 μm for Io. Europa and Ganymede decrease in albedo beyond 1 μm and Ganymede shows a minimum in albedo at 1.6 μm. Callisto was measured under poor observing conditions, hence no useful results were obtained.

As observing techniques have developed and as detector sensi-

tivity increases, the identification of water frost on Europa and Ganymede has been placed on a firmer footing. Pilcher et. al. (1972) and Fink et. al. (1973) obtained higher resolution spectra of 33 cm^{-1} and 25 cm^{-1} respectively using interferometers and fourier spectroscopy techniques (Vanasse & Sakai, 1967). Absorption due to water frost as measured in the laboratory (Keiffer, 1970) appear at 1.49, 1.55, 1.64 and 2.0 μm (figure 9). These absorptions are well defined for Europa and Ganymede and broad, weak features appear on Callisto at 1.52 and 2.05 μm (figure 10). Pilcher et. al. (1972) hypothesize that the decrease in absorptions from Europa and Ganymede and an even larger decrease for Callisto, may be due to a decrease in the frost-covered fraction of each satellite's surface. The high geometric albedo of Io (almost three times that of Callisto in the visible but similar to Callisto in the infrared) and lack of absorption bands, remains unexplained. Suggested mechanisms include small particle size on the surface producing higher reflectance which would in turn mask the absorptions. There are also, according to Pilcher et. al. (1972), variations in infrared reflectance on the leading and trailing sides of Europa and Ganymede which indicate 20% more frost on the leading side than on the trailing side of Ganymede and a 30% difference between the two sides of Europa.

Variations as a function of rotational phase in the infrared has been measured using the more sensitive InSb (indium antiminide) detector and four interference filters with band passes centered at 1.57, 2.27, 3.80, and 4.71 μm (Hansen, 1975). Unfortuneately the results are inconclusive due to poor rotational coverage. The significance of this

paper is that it agreed with a finding by Pilcher et. al. (1972) that there is a feature at 1.5 μm in Io's reflection spectrum which was not found by Fink et. al. (1973).

Laboratory Studies

Laboratory investigations are carried out to study the behavior of materials expected to exist on satellite surfaces from theoretical considerations based on cosmic abundances, stability of frosts (Lewis, 1972, 1973, 1974), (Watson et. al., 1963), (Lebofsky, 1975), Jupiter's past history and its effect on its satellites (Pollack & Reynolds, 1974), polarization measurements (Veverka, 1971) and post eclipse brightening (Binder & Cruikshank, 1964).

Keiffer (1970),for the first time investigated the behavior of CO_2 and H_2O frosts from .8 - 3.2 μm as mixtures. He made his measurements with an optical configuration of 0^o angle of incidence and a phase angle of 12^o commensurate with the maximum phase angle of Jupiter as seen from Earth. A smoked MgO standard was used to divide out instrument effects. Figures 9 and 11 show the reflection spectra of both H_2O and CO_2 frosts. As can be seen the spectra are dependent on textural scale which Keiffer found was related to the relative concentration of condensing gas at the frost surface. The relation is complex and a simple, quantitative relation of reflection spectra versus composition cannot be defined on the basis of the work done in this study. The effect of the presence of H_2O on the CO_2 absorption features is also a dominant factor. The intensity of the stretching modes at 3.1 μm is very strong and increases with texture, masking solid CO_2 features.

A number of reflection spectra of solids was measured by G.T. Sill (1973) in a paper entitled "Reflection spectra of solids of planetary interest." The spectra were obtained by illuminating the material at a 45^{o} angle of incidence and measuring the reflected light normal to the sample. The spectra are normalized to a LiF standard and include the spectral region from .2 - 2.5 μm. Included in his study are sulfur compounds, sulfates and iron chloride compounds. The samples were measured under a variety of conditions of temperature variations (dry ice and/or liquid nitrogen temperatures) and/or exposed to room temperature and UV radiation (Hg 2537 Å). The results of this work have not produced unique spectra for every mineral measured. It appears that in some situations materials of different chemical composition produce similar spectra because the spectral region covered is finite and the instrument response limits the observable variations.

A wider range of frosts expected to exist on satellites in the outer solar system were measured by Keiffer & Smythe (1974). They compared their laboratory spectra with those of the Galilean satellites in terms of position and shape of absorption features found in Europa's and Ganymede's spectrum. Included in their study were CH_4, NH_3, H_2S, NH_4SH and H_2O frosts. They note that these compounds will have migrated to the poles which act as cold traps and will be difficult to detect because of the viewing geometry. The fit for all frosts except H_2O is poor (figure 12). A temperature dependence inversely proportional to the depth of the 6100 cm^{-1} (1.6 μm) and flatness of the 4500 cm^{-1} (2.2 μm) feature was found. The best match for Europa's spectrum is

water frost at 150° K. The grain size found to be consistent with satellite spectra is on the order of .01 cm. This temperature determination disagrees with the temperature of 95 ± 10° K derived for Europa by Fink et. al. (1975) using the same feature. The discrepancy remains unaccounted for. However Fink et. al. took great pains to calibrate their temperature determination and empiracally define the relationship. Keiffer & Smythe's method of determination is not well defined and appears to be an observed agreement between laboratory H_2O frost at 150° K with one instrument and the spectrum of Europa and Ganymede measured with a different instrument. Fink et. al. divided the equivalent width of the 6056 cm^{-1} feature by that for the 6300 cm^{-1} (1.6 μm) absorption complex at different temperatures in the lab. A calibration curve consisting of the percent area ratio of 6056 cm^{-1}/ 6600 cm^{-1} feature versus temperature is the basis for their temperature determination of 88 ± 10° K for Ganymede and 95 ± 10° K for Europa. This measurement is probably reasonable provided it is the temperature of the frost alone, not necessarily of the whole satellite disk.

Other topics investigated by Keiffer & Smythe (1974) include placing upper abundance limits on materials from solid reflectance spectra. The width and intensity of dominant features such as the water frost bands prohibit defining other possible constituents which may be present. It should be noted that the optical set up was the same for this work as for Keiffer's (1970) original work. A subsequent paper published by Smythe (1975) dealt with the temperature dependence of gas hydrate frosts. These frosts which have "guest" molecules in an ice matrix or clathrate lattice, have a lower vapor

pressure and hence a longer lifetime on smaller satellites. The results show that the water features at 1.5, 1.6, and 2.0 μm dominate the spectra and prohibit the detection of any "guest" molecules at the resolution of 1975 infrared astronomical spectra.

Visible reflection spectra (0.3 - 1.1 μm) of irradiated H_2O, NH_3, H_2S, NH_4HS and their hydrates recently appeared in the literature (Lebofsky & Fegley, 1976). Figure 13 shows an H_2O frost reflection spectrum. As can be seen the spectrum is featureless and flat contrary to the visible spectra of the Galilean satellites (figures 5-8). The frost deposits on a stainless steel cold finger of NH_3, H_2S and NH_4HS and their hydrates are measured in reflected white and UV light. It is interesting to note the changes of sulfur-containing frosts after irradiation (figure 14). At about .6 μm there is an absorption which strengthens with exposure to UV irradiation and is attributed to S_5–S_7 sulfur diradical transitions. There is no indication how long the feature persists after the UV radiation is removed. Nash et. al. (1976) did similar experiments with various mixtures of irradiated compounds. The changes were temporal on the order of a few hours. If the sun affects the Galilean satellites in this way, a differement reflection spectrum should be seen upon satellite reappearance than before disappearance. As mentioned by Nash et. al. (1976) the difference should be in the form of a reappearance darkening which has not been reported. Investigations also need to be done on the effect of irradiated samples on the infrared region of the spectrum.

A recent laboratory investigation of mixtures of solid phases

was undertaken to model Io's surface composition to telescopic observations of Io, its unusually high albedo, absence of diagnostic absorptions and the discovery of sodium emission lines in its spectrum (Nash et. al., 1976). Considering cosmochemical arguments (Lewis, 1972, Fanale, 1974) and aspects of Io's reflection spectrum, they measured reflection spectra of various mixtures with varying particle size, packing density, temperature, composition and amounts of proton irradiation to determine a surface compositon model consistent with known chemical and physical properties of the satellite.

This paper best illustrates the need for accurate and consistent reflection spectra of the Galilean satellites. Figure 15 shows the measurements and errors of Io's reflection spectrum used for comparison with their laboratory measurements. The two spectra in the visible region represent the trailing and leading side of Io (Johnson, 1971). The infrared measurements are embarrassingly uncertain. More accurate measurements will be available soon due to new, more sensitive detectors. The best match of laboratory spectra with observational spectra of the Galilean satellites is with a mixture of 55% (by volume) free sulfur, 30% dehydrated bloedite ($Na_2Mg(SO_4)_2 \times H_2O$), 15% ferric sulfate ($Fe_2(SO_4)_3 \times H_2O$) and trace amounts of hematite. Other combinations of minerals were compared with Io's reflection spectrum, most of which had features in the infrared which do not occur in Io's infrared spectrum. The other area which is also difficult to duplicate in the lab is the absorption edge and slope in the ultraviolet region of the spectrum. The effect on these samples due to the following properties was also investigated: temperature, particle size, packing density, and

the effect of low energy proton bombardment (5 kev) which is proposed to simulate Jupiter's magnetosphere and its interaction with Io. The effects of these parameters are summarized in a table (Table 1), shown here as an example of systemmatic investigations of solids.

INSTRUMENTATION AND DATA REDUCTION

The vidicon spectrometer consists of an optical system placed between the telescope and a silicon vidicon detector. The spectrometer section (Figure 16) consists of a reflecting entrance slit, a guiding eyepiece and photography section where guiding is done by viewing the absence of the object from the reflection around the slit. A spherical mirror reflects the light into one of two aluminum-backed prisms. The dispersed light is reflected through two more mirrors and onto the vidicon detector. The prisms are switched by a motor.

The detector is an array of backbiased diodes which lose charge with an influx of light. An electron beam scans the array recharging the diodes after an exposure. By measuring the current needed to recharge the diodes at a given position, the light intensity is measured. It has been determined, and is tested before each run, that the charge loss for each diode is proportional to the photon flux. Similarly, the recharge current is proportional to the charge lost. The raw image consists of 250 by 256 elements. The signal is converted to digital signal and recorded on magnetic tape. The image of the spectrum covers an area of about 20 by 256 elements. Figure 17 schematically shows the components of the vidicon system. For more detailed descriptions of vidicons the reader is referred to McCord, Bosel and Frankson (1975).

The observations were made on the night of November 18-19, 1975, at the 203 cm. (80 in.) telescope of the Mauna Kea Observatory at one

orbital phase of each satellite (Table 2). The observing sequence consisted of a wave-length calibration exposure for one prism with dispersion from .32 - .36 μm followed by two or more exposures of a satellite. The prism is switched, satellite exposures are made, followed by a wavelength calibration for the second prism, which covers the region from .53 - 1.06 μm. The calibration source is a Ne-Ar lamp with emmission lines (Figure 18) measured in the lab with a Heath monochrometer. Dark fields are recorded every one to two hours. An exposure of the uniformly illuminated slit in the spectrometer was made once for each prism during the run. It is used to remove the effects of irregularities along the length of the entrance slit, by dividing it into each image exposure.

The vidicon spectrometer was used primarily to test the instrument. It has a few advantages over the conventional filter photometer in that a higher wavelength resolution is attained using prisms. All wavelengths covered by one prism are measured simultaneously. This saves time at the telescope and produces more accurate spectra by reducing the number of different airmass corrections which have to be made. The vidicon detector is also sensitive from .32 - 1.06 μm, a spectral range achievable only with two separate photomultipliers. Using two prisms which are rapidly interchangeable is more efficient than changing photomultipliers. The vidicon also has a spatial dimension which is not available with conventional photomultipliers. This aspect provides a limited advantage with objects of small angular diameter because the spectrum covers only a few rows of the vidicon, but is useful for close objects such as the moon.

The quantity I want to extract from these measurements is spectral reflectance. The reflectance is derived from the satellite/star flux by way of the equation $(F_{sat}/F_{star}) \times (F_{star}/F_{Sun}) = F_{sat}/F_{Sun}$. The flux is expressed as $F_{sat} = [f(\lambda)\ S(\lambda,r,t)\ a\ (\lambda,r,t)]$. When the two fluxes are divided and the atmospheric transmission function, $a(\lambda,r,t)$, is the same for both satellite and star, this function cancels. This is the case for observations here, where the satellite flux is divided by star fluxes measured at the same air mass. Temporal transmission effects are assumed to be negligible. $S\ (\lambda,r,t)$ is the instrument response function of the telescope, spectrometer and vidicon. Since this is the same for all observations, it cancels when relative measurements are calculated. It is assumed the instrument is constant over time, (t). There appears to be a position dependence, r, on the vidicon target which does not divide out. Some of the measurements are unusable for this reason. I will mention this problem again in discussing data reduction procedures.

To produce the F_{sat}/F_{star} value the following steps are taken:

1. Subtract a dark frame from each image frame.
2. Print out approximately 50 rows of image frame to verify and locate the image.
3. Visually determine the spatial extent of the image (# rows) and the spectral extent (columns at which the signal begins and ends or becomes saturated).
4. Divide by a flat field image.
5. Average the rows of the object signal and save as a vector.

6. Perform a wavelength calibration.
7. Scale each intensity vector to a constant time interval (ten seconds was used in this study).
8. Average together the images of the same object or star.
9. Scale the blue and infrared star images to one arbitrary value which has the effect of making a continuous spectrum from .33 - 1.06 μm.
10. Divide object image by star image taking into account any wavelength shifts due to switching the prisms.
11. Normalize object/star ratio to .5667 μm.
12. Multiply object/star x star/sun flux.

Specific problems arose for these observations which necessitated the following departures from the above reduction procedures.

For some as yet unknown reason, the dark field exposure yields larger data numbers than the unexposed region of an image frame. The dark field consists of the image making procedure described by McCord and Frankston (1975) with an exposure time of 0 seconds. There is some mechanism which produces higher signal with a 0-second exposure than with a longer exposure. Further testing is needed to understand this phenomenon. To compensate for this larger dark subtraction, I averaged an area the width of the spectrum, both above and below the spectrum. This residual represents the excess subtracted from the spectrum. It is then added back to each row of the spectrum image.

Additional problems were encountered when ratioing images from

different areas on the vidicon. There is a wavelength and spatial dependent response. Unless the object and star are exposed on the same area of the vidicon, it does not divide out. More tests are also necessary to understand this problem. No correction could be made and the data beyond .8 μm was not used for Ganymede and Callisto measurements because of a false feature. This feature is definitely an artifact because it is also present in some star/star ratios, which should be unity.

In step 10, one must take into account a possible shift in wavelength correspondence with the horizontal vidicon elements (columns). For infrared measurements the shift was taken into account by a computer program which matches the position of the .76 μm telluric O_2 absorption and shifted the numerator image accordingly. A steep but small emission followed by an equally steep absorption in this spectral region is caused by the failure of the feature to completely divide out. Similar saw-toothed features which are larger than the noise level appear at the .92 μm water band and are not real. The blue images were matched by shifting the columns according to the positions of the emission peaks in the respective wavelength calibration images.

Wavelength calibrations are usually performed early in the reduction process. The dispersion constants, K, S_o, L_o for each prism have been determined from laboratory measurements by projecting monochromatic light onto the vidicon target. From the position on the vidicon of groups of three wavelengths in terms of column element, the constant

$$S_o = -c_1 + \frac{(\lambda_2 - \lambda_3)(c_2 - c_1)(c_3 - c_1)}{(\lambda_1 - \lambda_2)(c_3 - c_2) - (\lambda_2 - \lambda_3)(c_2 - c_1)}$$

$$K = (\lambda_1 - \lambda_2)(c_1 + S_o)(c_2 + S_o) \text{ and } L_o = \lambda_1 - K/c_1 + S_o).$$

where c_1, c_2, c_3 are column elements representing position on the vidicon. These values are calculated for as many possible groups of wavelength and position. The dispersion function, $\lambda = L_o + K/c + S_o$ is used to test the accuracy of the constants. The best values arrived at for the blue prism are $K = -89.7$, $S_o = -500.37$, $L = 0.1490$, and for the near infrared, $K = -118.80$, $S_o = -382.80$, and $L = .2230$.

During an observing run the scanning area of the target is set which determines the number of elements (256) per millimeter. The position of the spectrum also changes by a column or two as the prisms shift slightly due to the position of the telescope and motion when the motor switches the prisms. For this reason a calibration exposure must be made with each prism change. These factors impose a linear offset in the dispersion constants, which is calculated from each exposure of the Ne-Ar light source using the following relations:

$$K' = K \times (C_1' - C_2'/C_1 - C_2); \; S_o' = [S_o \times (C_1' - C_2'/C_1 - C_2)] - C_1' + [(C_1' - C_2'/C_1 - C_2) \times C_1]$$

where C_1, C_2 are column elements for any two wavelengths calculated using the characteristic prism constants above, and C_1' and C_2' are the observed column elements for the same two wavelengths.

Error Analysis

There are three sources of error in these measurements, instrumental accuracy, wavelength calibration and the error in the star/sun reduction.

Figure 19 shows images divided by themselves from two different exposures. The results are close to unity as they should be. The deviations show the repeatability of the instrument over short time intervals. The effects of dividing two images of the same object over long time intervals is not available from these observations because of the problem with images recorded on different parts of the target. By coincidence those images recorded higher on the target were recorded later in the night. The short term repeatability looks very good to about 1.0 μm. The effects of the reduced spectral response of the vidicon are evidenced by the fluctuations at the infrared edge of the spectrum (19c). In figure 19a, the blue end of the spectrum shows a lot of noise on top of a slope created by the change in air mass. In the satellite reflectance measurements the difference in air mass between satellite and star was not more than .02 air masses and in most cases less than that. Table 2 lists the air mass at the time of each satellite measurement with the air mass at the time of the respective star measurement. In most cases the air masses could be matched closely.

The wavelength calibration is determined by the dispersion function which assigns a wavelength to each element of the target. The width of the entrance slit determines the spatial resolution. The target is 2.5cm from edge to edge with 10 elements/mm. The slit width was

.3mm which puts the spatial resolving limit at 3 elements if the width of the target is scanned. If the slit width were smaller, the resolution would be better and more of the dispersing power of the prisms could be used. We opened the slit, however, so as not to lose light from differential refraction in the atmosphere. Therefore, in the blue region from .33 - .50 μm the wavelength resolution is .0018 - .0036 μm. This resolution decreases between .45 - .65 μm to .0036 - .0050 μm and between .65 - 1.06 to .0036 - .0120 μm. This is still higher than the .0250 μm standard wavelength interval for the filter photometer.

The errors in the star/Sun ratio, 10 Tau/sun (table 4) constitute the largest contribution to the total error in the measurements. Table 5 lists the interpolated values from Table 4. The errors listed in Table 4 represent the standard error of the mean (standard deviation divided by $\sqrt{N}$) which is the range within which the mean of the observations can be expected to vary. The errors are usually less than 1%.

The star/Sun ratios used in this work are from Owensby et. al. (1977) which were calibrated using observed values of 10 Tau/Alpha Lyrae and the Alpha Lyrae/Sun flux determined by Nygard (1975). This new standard Alpha Lyrae/Sun flux differs from previous standards in that the calibration is made from a lunar standard, Apollo 16 and multiplied by the laboratory reflectance of Apollo 16/MgO. The assumption that MgO/Sun = 1 is made and $(^{\text{Apollo}}_{16})_{\text{telescope}} / (^{\text{Apollo}}_{16})_{\text{lab}} = 1$. From

$$\left(\frac{\text{Alpha Lyrae}}{\text{Apollo 16}}\right)_{\text{telescope}} \times \left(\frac{\text{Apollo 16}}{\text{MgO}}\right)_{\text{lab}} = \frac{\text{Alpha Lyrae}}{\text{Sun}}.$$

Interpolating these new photometer calibrations for use with the vidicon spectrometer seems to be a valid procedure. The best evidence for this is the coincidence of measurements of the asteroid Vesta made with the photometer and the vidicon spectrometer (McFadden et. al., 1977).

Figure 20 shows the effect of multiplying satellite/10 Tau by the interpolated 10 Tau/Sun. The correction is mostly one of slope. The blue Io/Sun reflectance (20a) was not available when these figures were made. The gaps in 20 b, c, are from lack of adequate overlap between the two prisms. It was not necessary to show Europa/Sun and Europa/10 Tau because the differences are systemmatic for all four satellites.

RESULTS

In figure 5-8 three sets of observations are compared for each of the four satellites. The different measurements do not coincide well. Johnson (private communication) suggested that his measurements be recalibrated using improved star/Sun ratios. This was done in figure 21 using the calibrations of Elias (1972) and that of Pieters & Owensby (Owensby et. al., 1977). The .38 μm data point was deleted from the calculations using Elias's calibration because the value is unrealistically high. The high reflectance at .9μm looks like it might be due to the star/Sun calibration but it is in Johnson's measurement of satellite/Alpha Leo. If the .9 μm data point is ignored the effect of recalibration (figure 22) is to bring the near infrared reflectance down closer to the measurements of Wamsteker and McFadden. A systematic positive slope from .7 - .95 μm is removed from Johnson's reflectance by this recalibration. The fact that the three sets of measurements do not agree should be considered in light of the fact that Johnson's results represent the average of very good rotational coverage whereas Wamsteker's results and those presented here came from measurements made at essentially one orbital phase.

The new measurements presented here for Io show the steep absorption edge beginning at .5 μm (or .6μm depending on the point of view), the shallower absorption between .5 and .65 μm is also present. From the peak reflectance at .7 μm the reflectance decreases about 20% to 1.06 μm. There are no features beyond .7 μm.

Europa has a less steep absorption edge and a shallower .5 - .65 μm absorption feature. Its peak reflectance is at .7 μm but is 5% smaller than Io's feature at that wavelength. The decrease in reflectance toward the infrared edge is also 20% of the peak reflectance.

The ultraviolet absorption edge of Ganymede is of comparable strength to that of Europa. There appears to be a few narrow, weak absorptions at .4 μm and .5 μm. Since they do not appear in Io and Europa's spectrum they probably are real. The existence of these features should be further investigated. They might be caused by the column shift which is necessary to match wavelength when dividing two images. Due to a lack of wavelength overlap between the two prisms it is difficult to describe the .5 - .65 μm absorption. In previous measurements the absorption is present but to a lesser degree than in Io's and Europa's spectrum. It appears as though the slope between .5 - .65 μm is steeper in Ganymede's spectrum than in Io and Europa's but the absorption depth is not necessarily greater. The data beyond .8 μm is not usable for Ganymede and Callisto because of the spatial problem on the vidicon. (see data reduction section).

The ultraviolet absorption in Callisto's reflection spectrum is approximately the same strength as that of Europa; it is stronger than that of Ganymede. The small, narrow-band absorption band does not appear, instead the absorption edge begins at .65 μm and the slope is less steep than Io, Europa or Ganymede's spectrum.

The ultraviolet absorption is either progressively masked by some material from Io to Callisto or there is some material causing

the absorption which is present in progressively greater quantities from Callisto to Io. The .56 - .65 μm absorption is present in many planetary objects but it cannot be attributed to one mineral. The fact that it appears with different strengths in different satellite spectra confirms that the feature is not an artifact of the reduction proceedure. The decrease in reflectance toward the near infrared, which begins at .7 μm for all the satellites (this happens in Ganymede's and Callisto's spectrum according to Wamsteker's measurements) is inconclusive until the behavior of the spectra beyond 1.0 μm is known with more precision. It is significant that the ultraviolet absorption edge is at the same wavelength for all four satellites at the observed orbital phase. The position of the edge is temperature dependent and is observed to vary for the leading and trailing side of Io (Nash & Fanale, 1976).

Satellite/satellite ratios provide a good means of comparing spectra. Their errors are free of the star/Sun calibration uncertainty. Figure 23 a, Io/Europa, shows the difference in the strength of the .5 - .65 μm absorption and shows an absorption wing to .7 μm. The difference in ultraviolet absorption depth shortward of .5 μm is still extreme, and would not be noticed as much by visually comparing the two satellite/Sun measurements. Toward the infrared, beyond .7 μm, the albedo difference is shown by the slight slope toward 1.0 μm. It is difficult to say whether the upturn at 1.0 μm is real or an instrumental response.

In figure 23 b, the fact that Ganymede has a stronger ultraviolet absorption is emphasized by the negative slope. The .5 - .65 μm

feature is the same for both satellites and the slightly decreasing slope exists beyond .7 μm. The bump at .9 μm is the artifact resulting from exposing images on different portions of the vidicon.

Callisto has less of a difference in the strength of the ultraviolet absorption. Again the .9 μm artifact is present.

Conclusion

The existing spectral reflectance measurements obtained by three different observers, at different times and with different instruments, do not provide the fundamental, experimental base needed to interpret the spectra. Theoretical investigations into the cause of the spectal features is also necessary before additional interpretations can be made (Johnson, private communication). For these reasons, more visible and near-infrared observations are needed. The observed variations with orbital rotation (Johnson, 1969) should also be redocumented in future observations for the completeness of the observational data.

figure 1

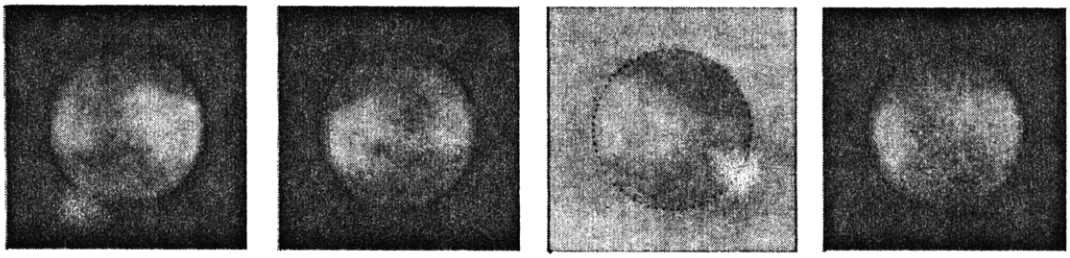

figure 2

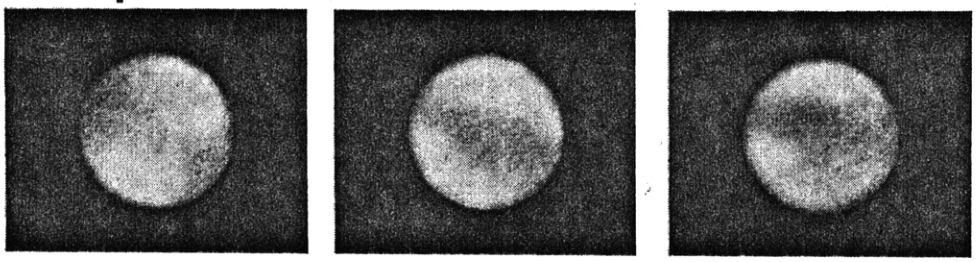

figure 3

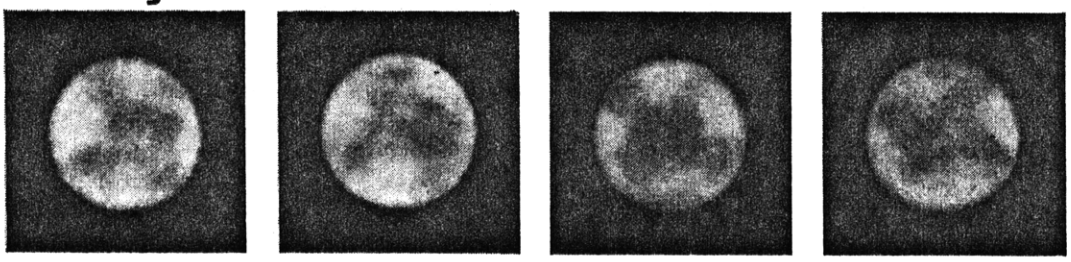

figure 4

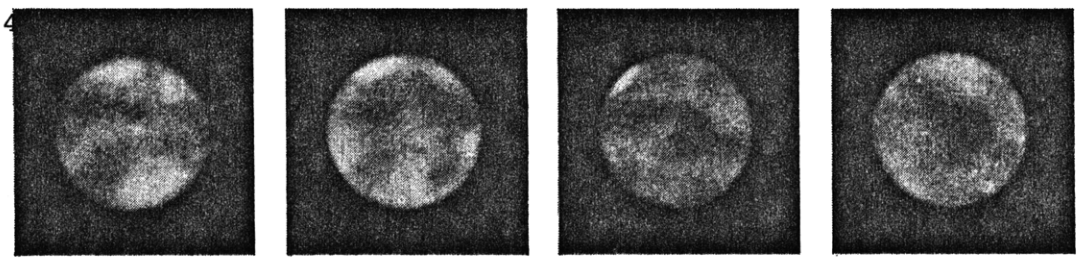

FIG. 1. Selected satellite drawings by the author made with the 108cm reflector at Pic-du-Midi Observatory in yellow light during September 1973. Central Meridian longitudes are given. South is at the top.

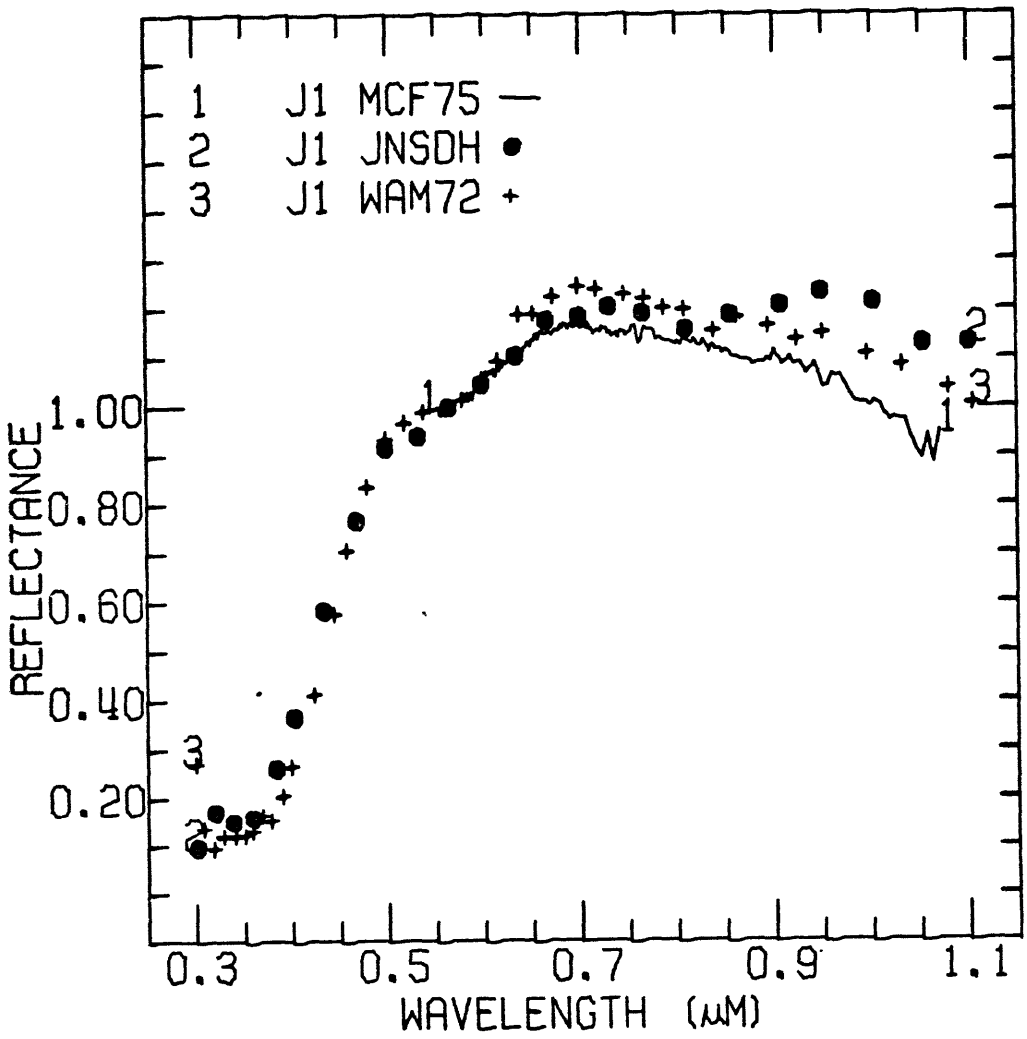

figure 5

Galilean satellite spectral reflectivity as measured by McFadden, 1975 (MCF75), Johnson, 1970 (JNSDH), and Wamsteker, 1972 (WAM72).

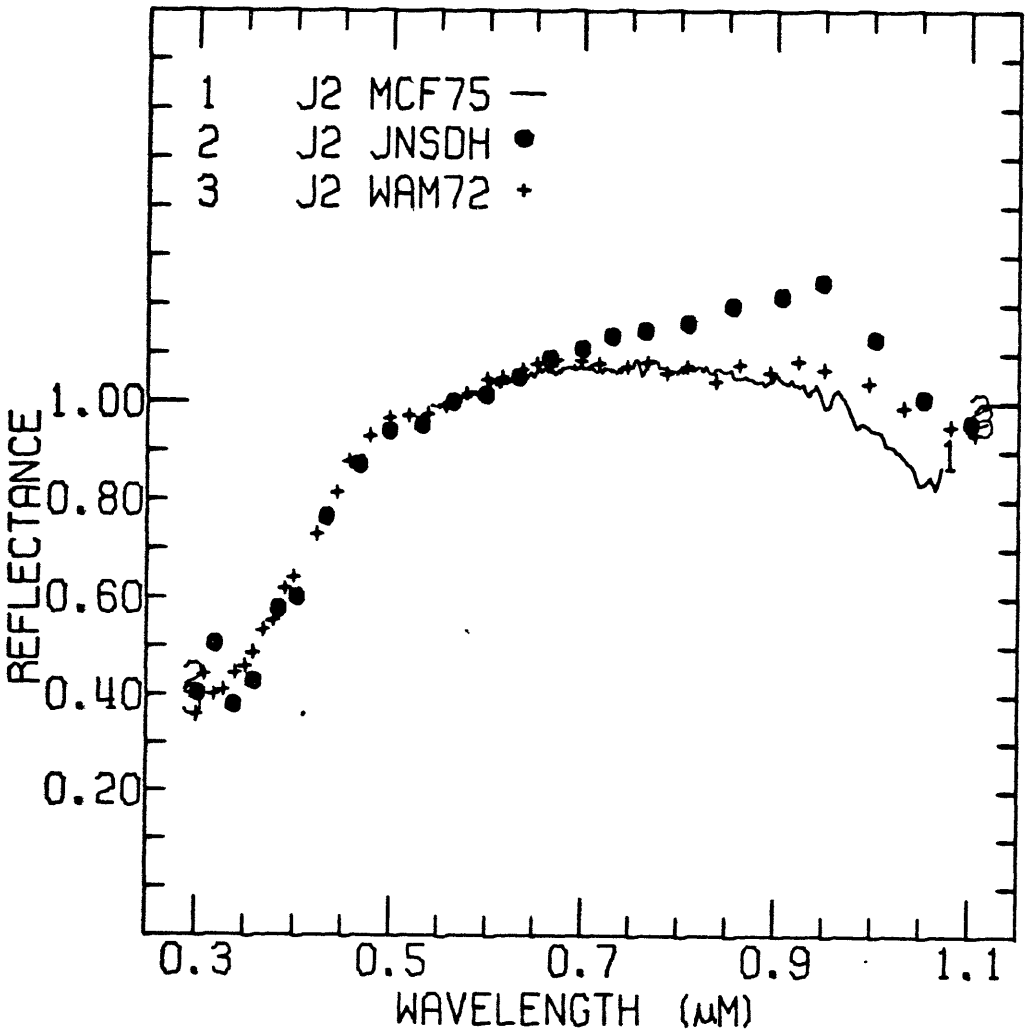

figure 6

Galilean satellite, Europa, as measured by McFadden, 1975, Johnson, 1970 (JNSDH) and Wamsteker, 1972 (WAM72).

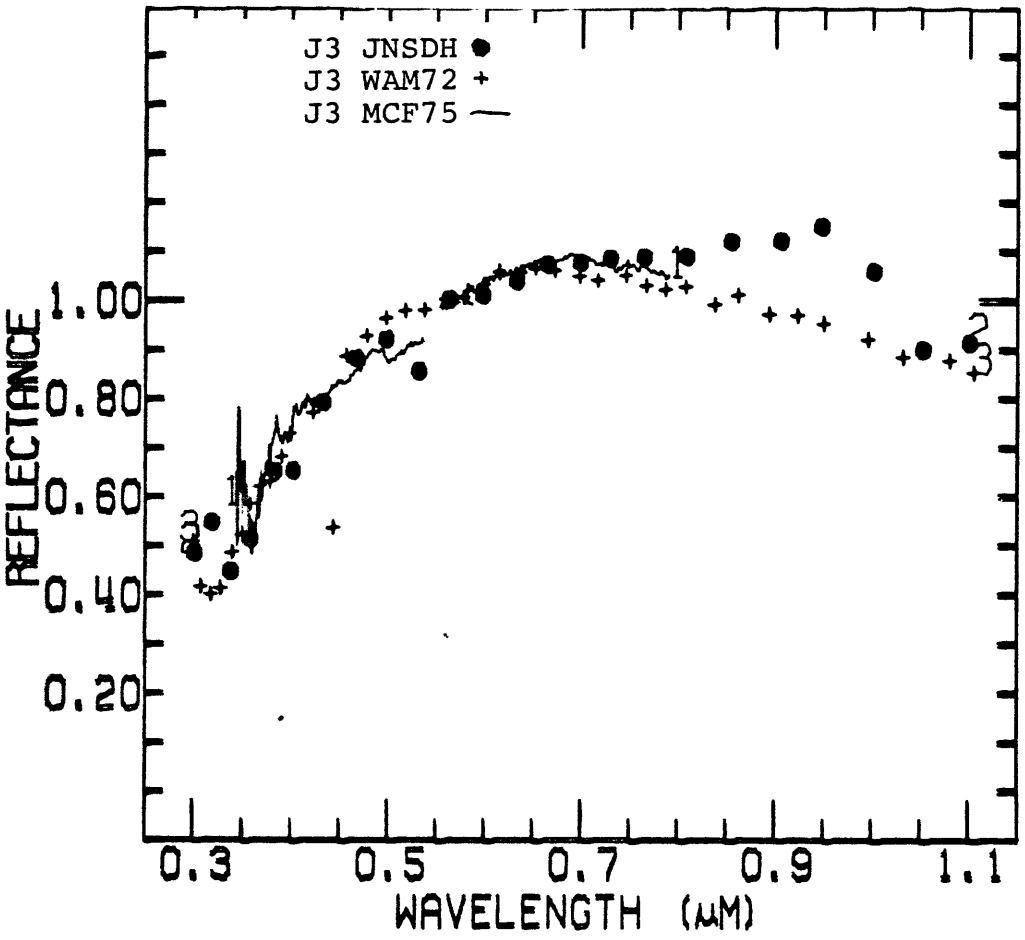

figure 7

Galilean satellite, Ganymede as measured by McFadden, 1975, Johnson, 1970 (JNSDH), and Wamsteker, 1972 (WAM72).

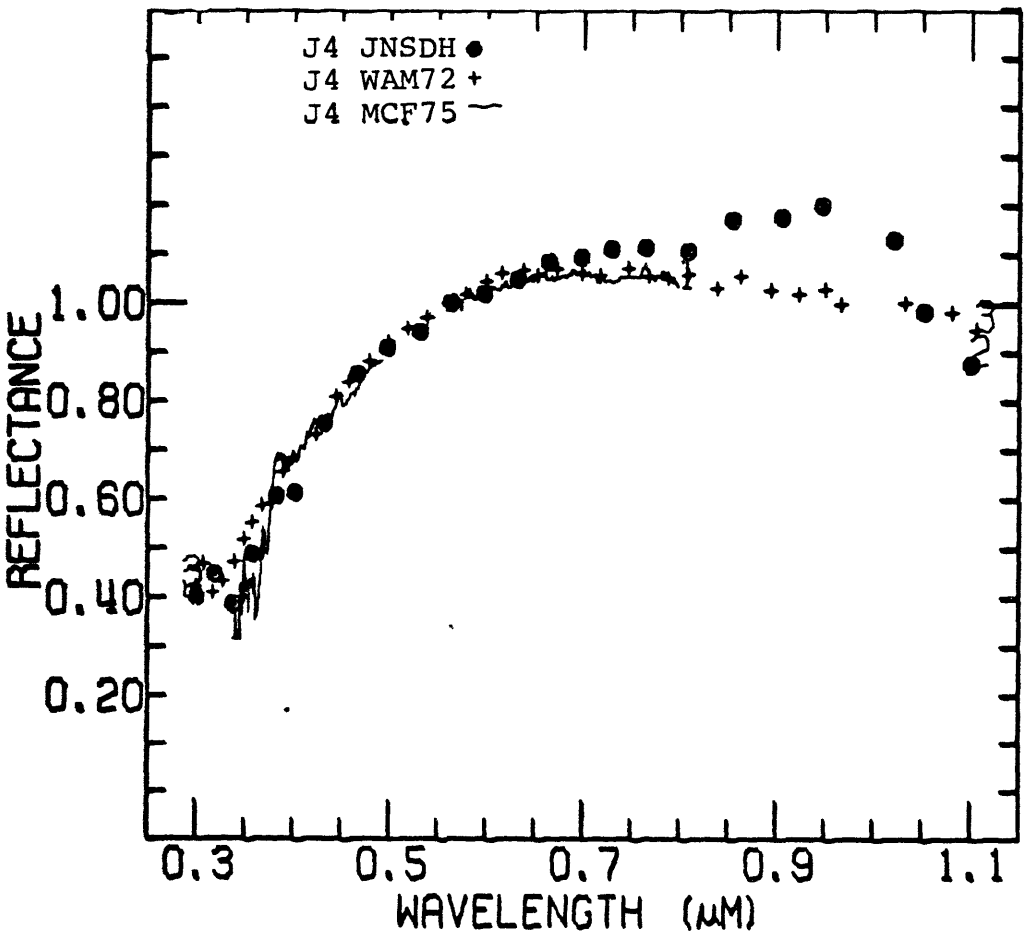

figure 8.

Galilean satellite, Callisto as measured by McFadden, 1975, Johnson, 1970 (JNSDH) and Wamsteker, 1972 (WAM72).

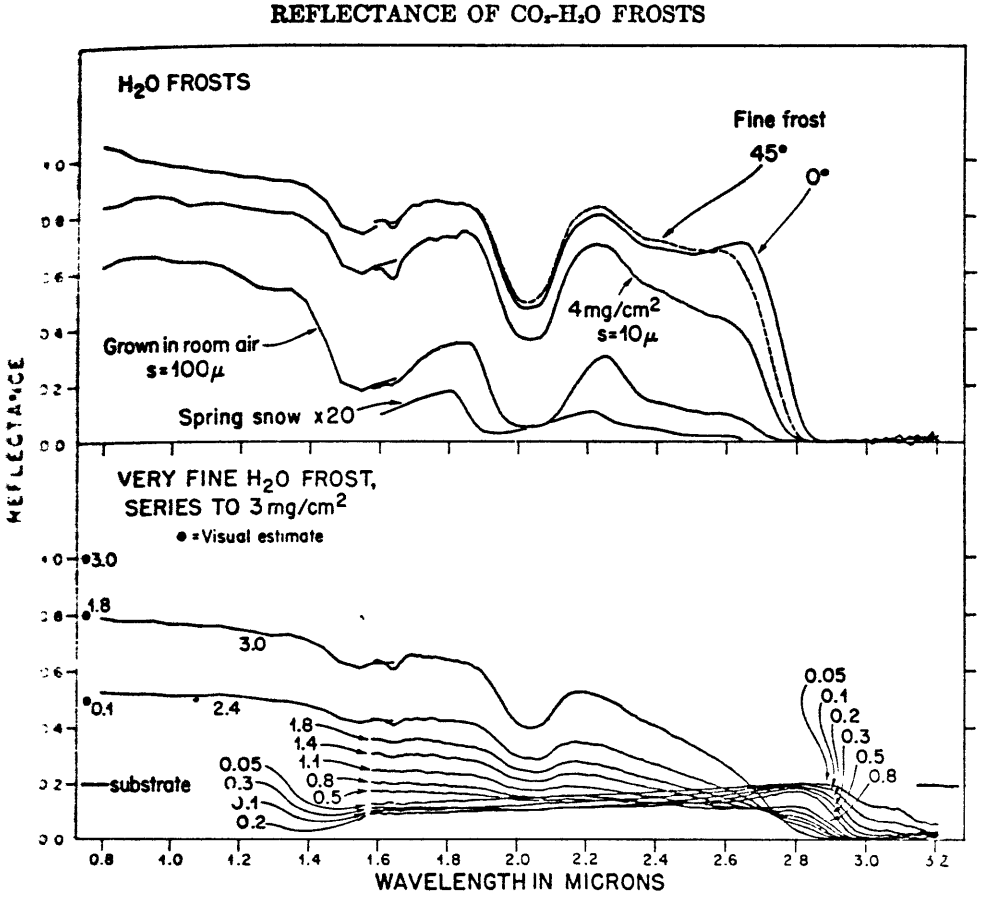

Fig. 2. Spectral reflectance of H_2O frosts. s is the textural scale. The snow and air temperatures were 0°C and 9°C for the undisturbed natural sample.

figure 9

Spectra of laboratory water frost, from Kieffer, 1970.

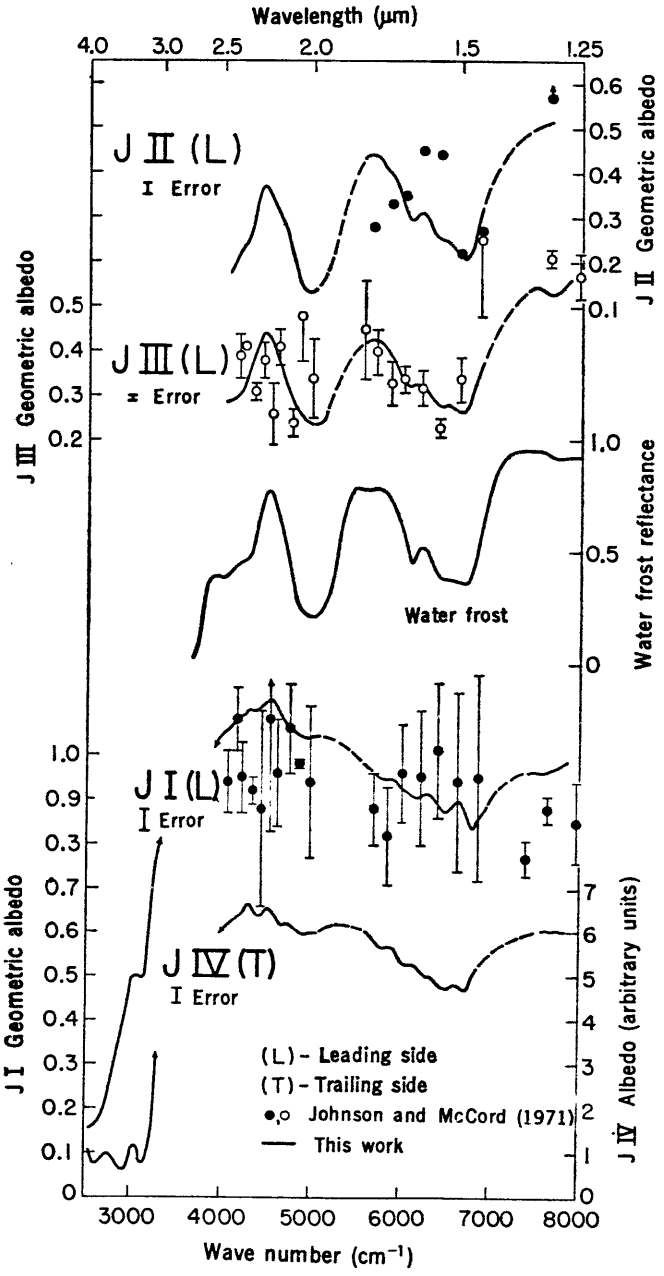

figure 10

Reflectivities of the Galilean satellites identification of water frost, from Pilcher et.al. 1972.

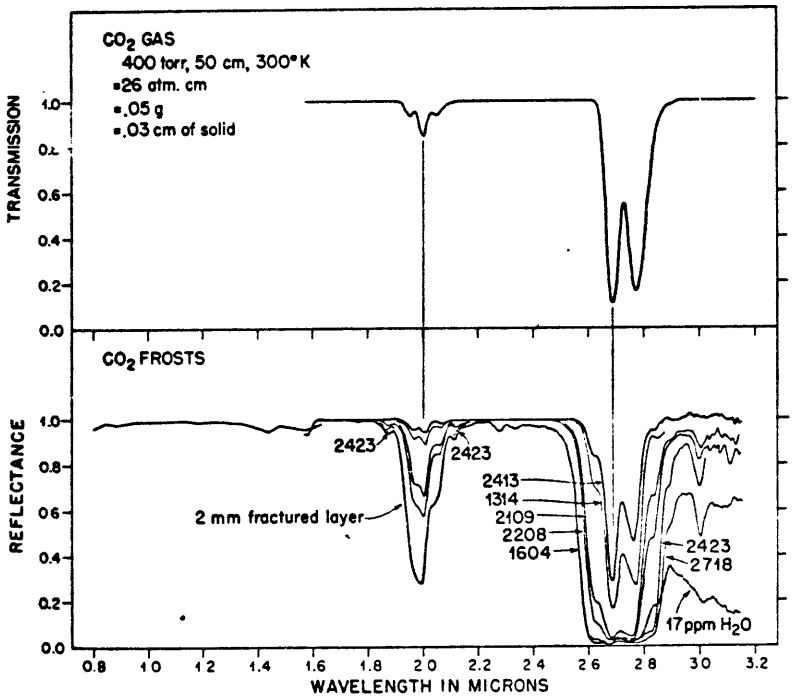

Fig. 1. Spectra of CO_2 gas and frosts. The finest sample precipitated from a cloud. The coarsest samples grew as closely packed columns. A typical example is shown of the low reflectance observed near 3.1 μ for commercial high-purity CO_2.

figure 11

Spectra of CO_2 frosts from Keiffer (1970).

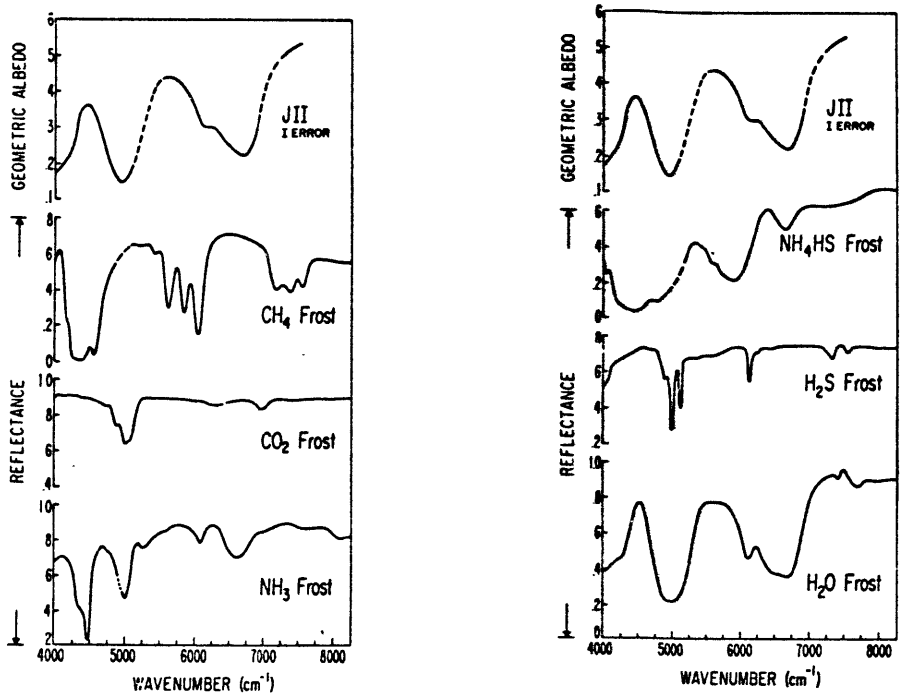

FIG. 1. Spectra of Europa (JII) and the laboratory frosts. The satellite spectrum is dashed across the regions of strong telluric absorptions. All these laboratory spectra were obtained at 77°K. The mean grain size of the laboratory frosts were approximately 0.2, 0.005 and 0.01 cm for NH_4HS, H_2S and H_2O respectively. The mean grain size of the laboratory frosts were approximately 0.001, 0.03, 0.05 cm for CH_4, CO_2 and NH_3 respectively. The CH_4 sample could not be grown optically thick because of the small temperature margin below the triple point; the original data have been multiplied by 2.5 to account for this.

figure 12

Spectral reflectivity of Europa compared with different laboratory frosts. Keiffer & Smythe 1974.

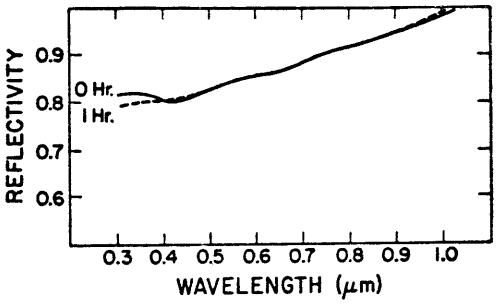

FIG. 2. H_2O frost reflection spectra.

figure 13

Visible H_2O frost reflection spectrum from Lebofsky & Fegley, 1976.

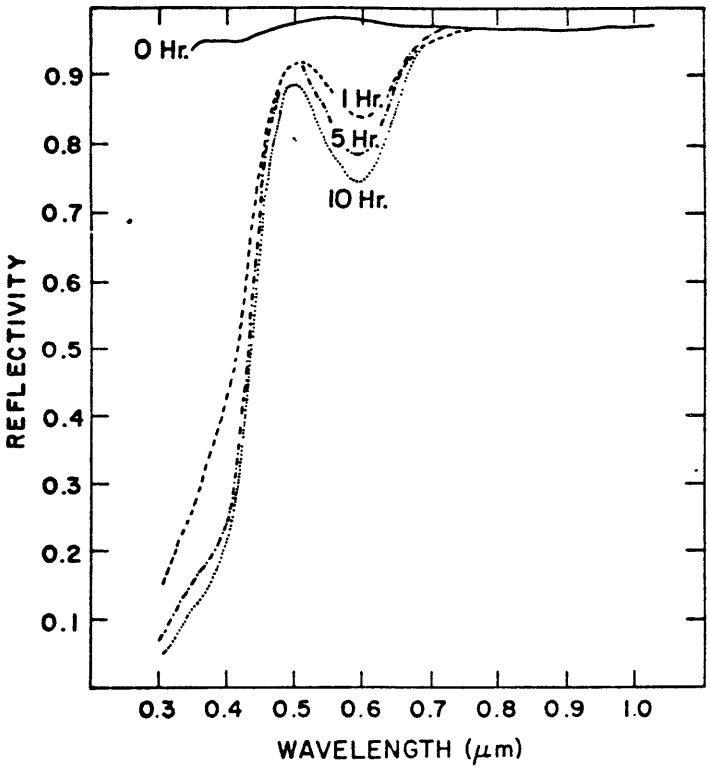

FIG. 5. H_2S frost reflection spectra.

figure 14

H_2S frost reflection spectra at different time intervals from exposure to UV irradiation

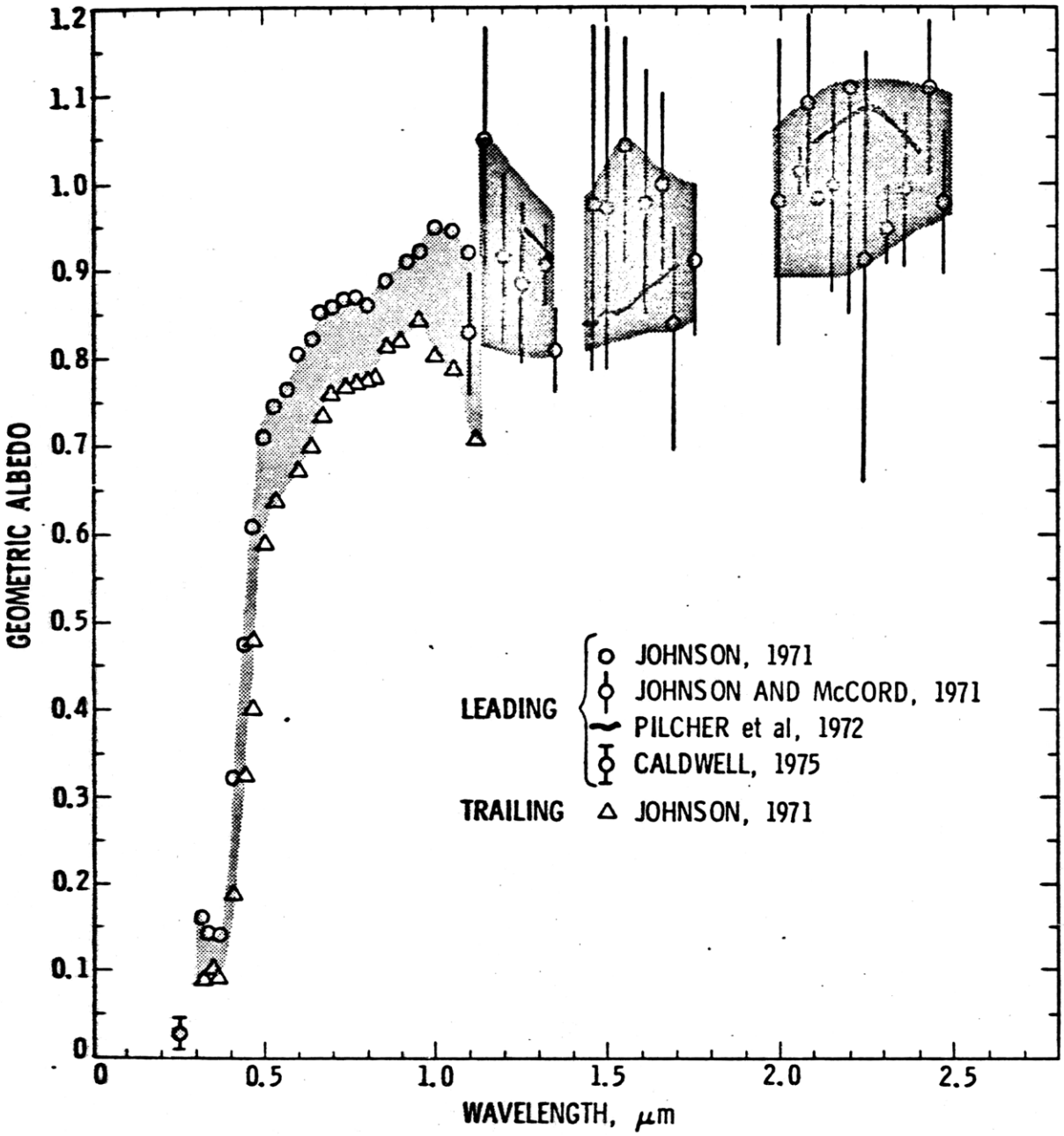

Io's reflection spectrum, Nash & Fanale 1976, used for comparison with laboratory work.

FIG. 15

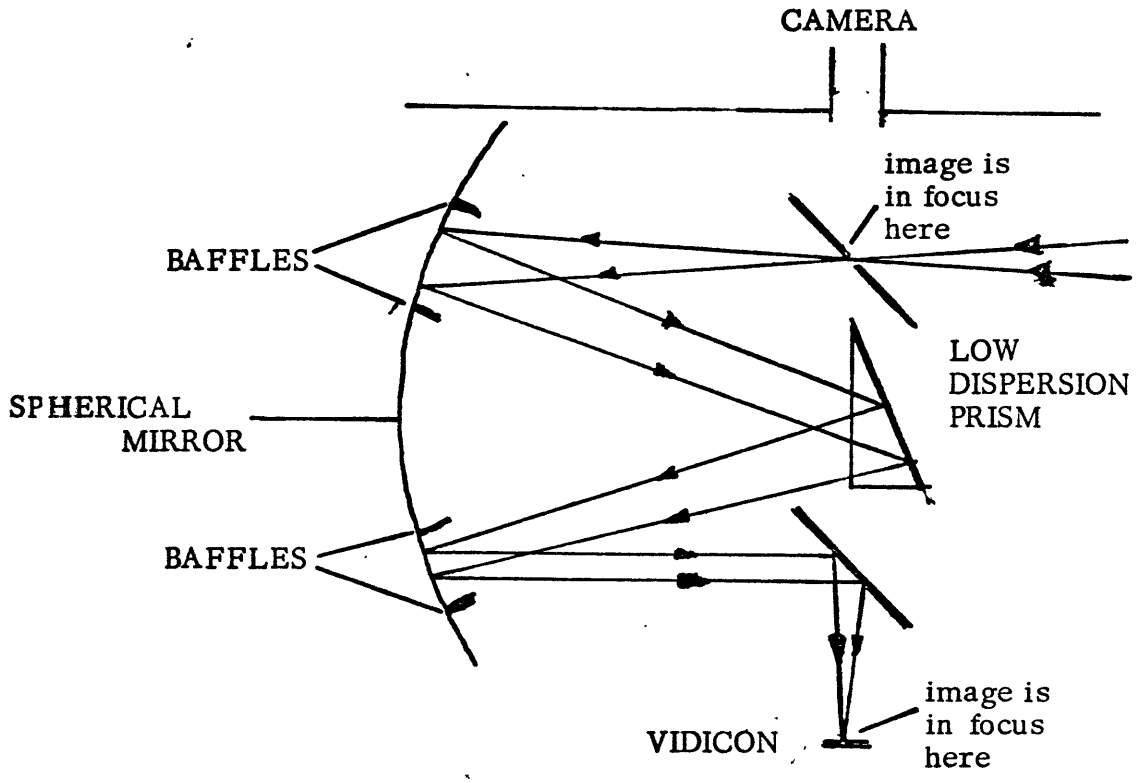

Figure 16 Optics of the MIT RSL vidicon spectrometer. The telescope is to the right.

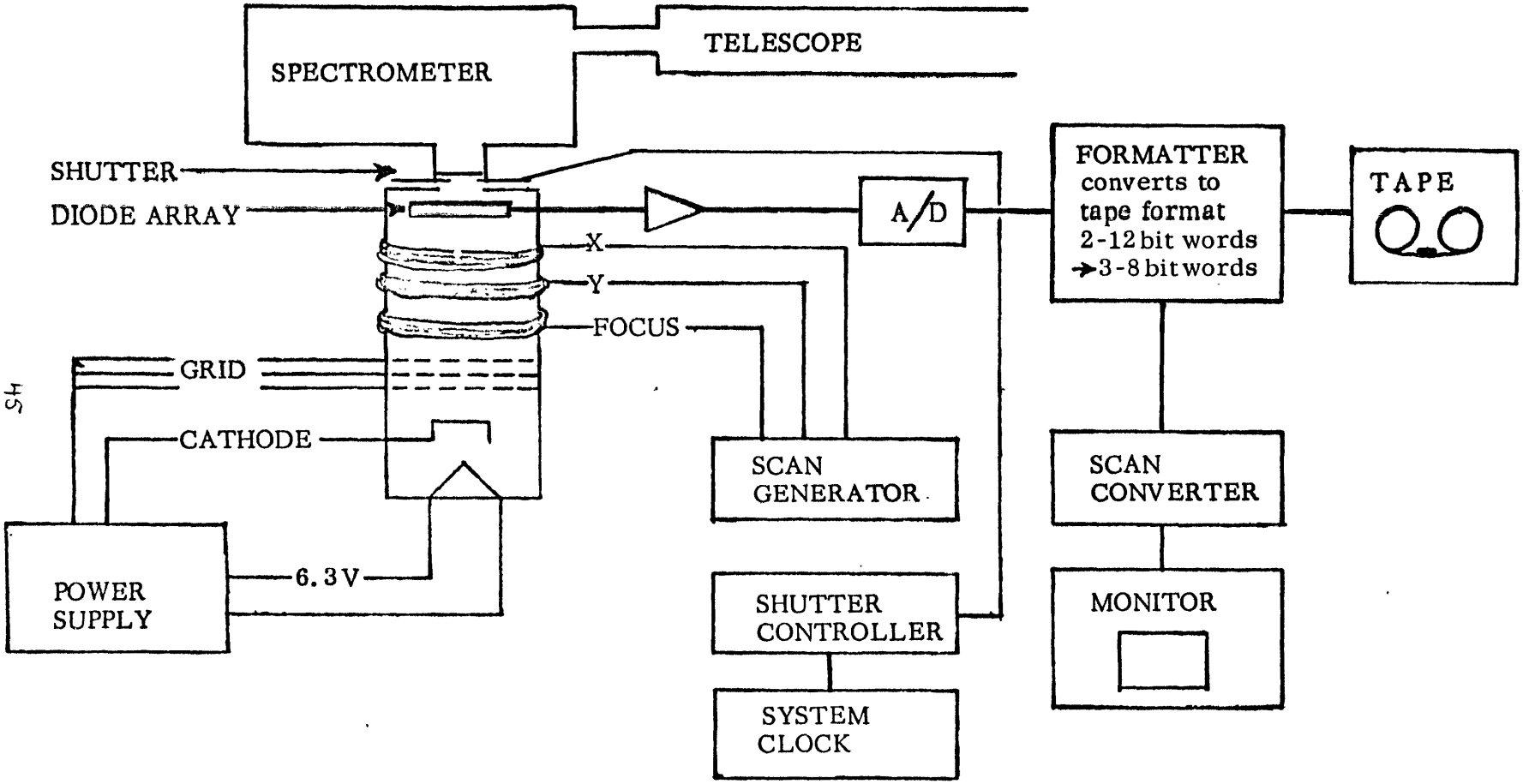

Figure 17 The MIT$_{RSL}$ vidicon system with the spectrometer attached.

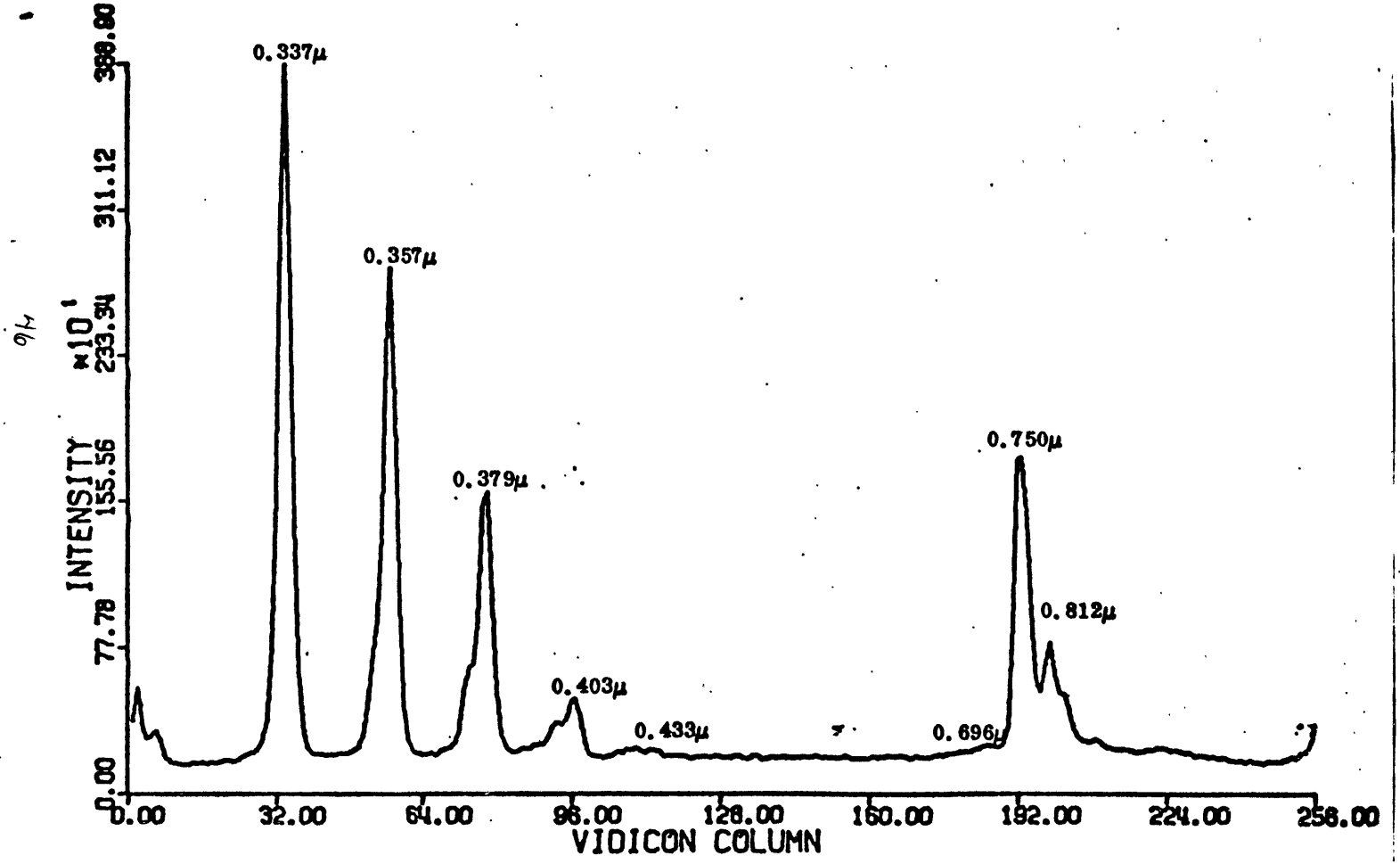

Figure 18 A spectrum of the calibration source, indicating vidicon intensity of each vidicon element along one row. Assigned wavelengths are indicated.

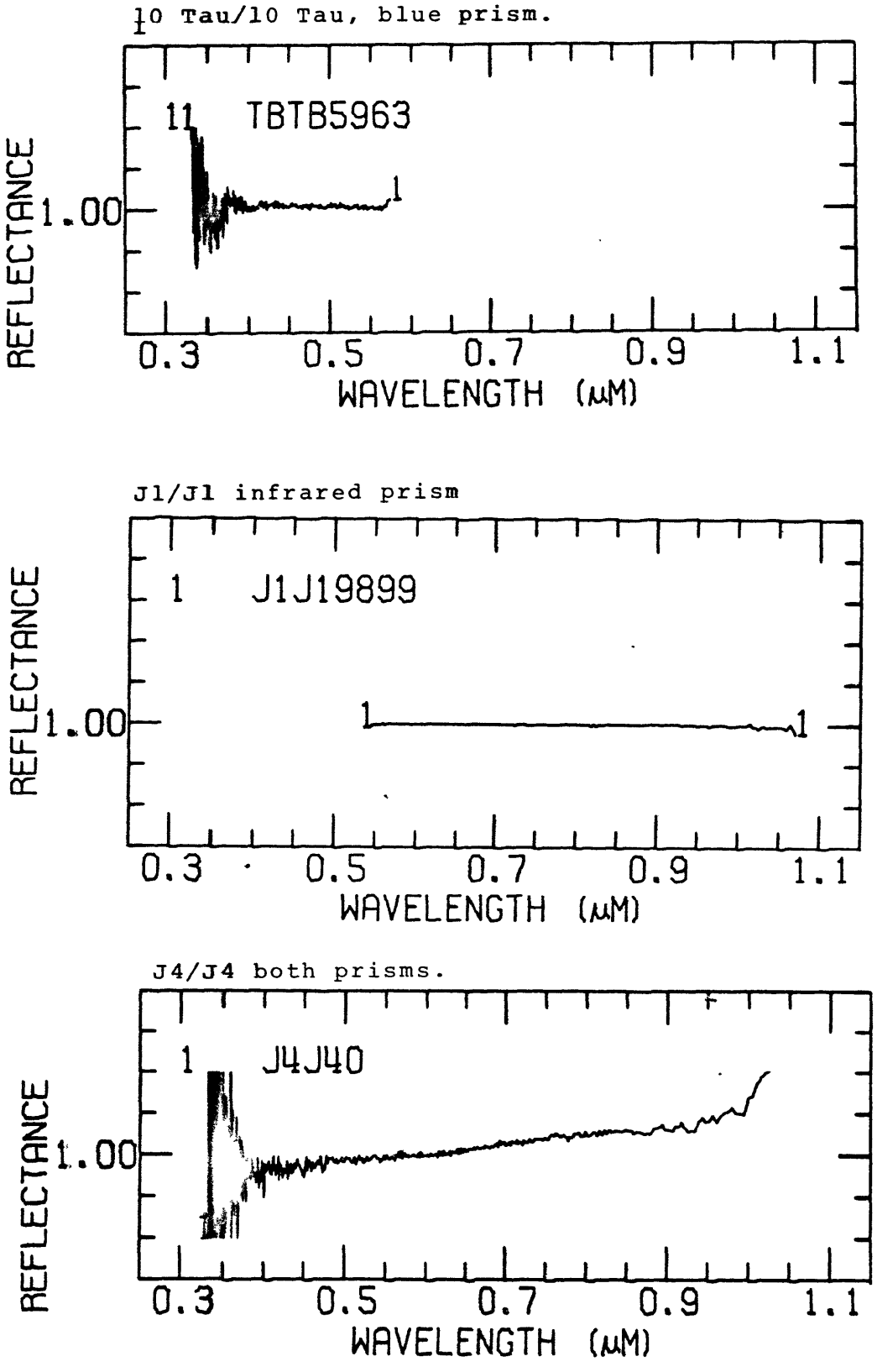

figure 19 a,b,c

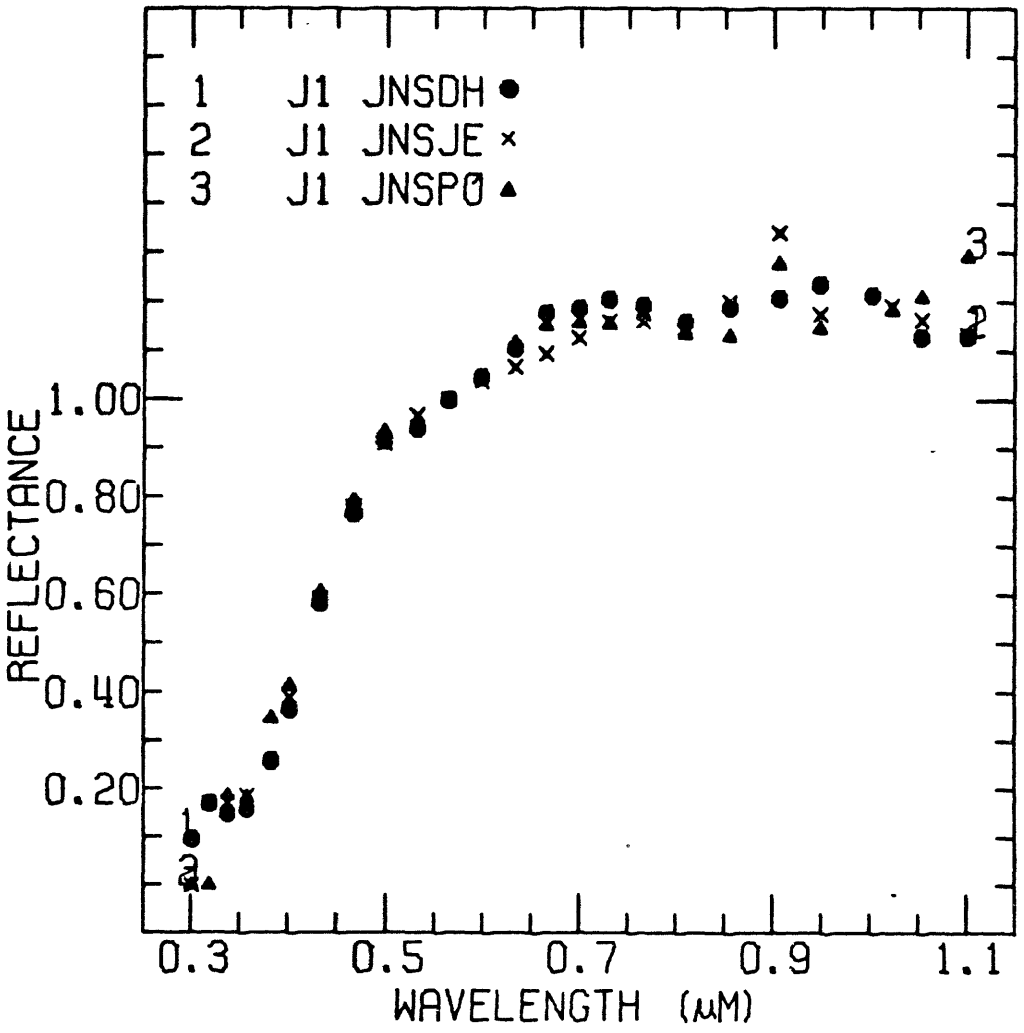

figure 22 a

Three star/ Sun calibrations, Johnson, 1970 using standard star of D. Hayes (JNSDH), J. Elias (JNSJE), and Pieters, Owensby et.al. (JNSPO).

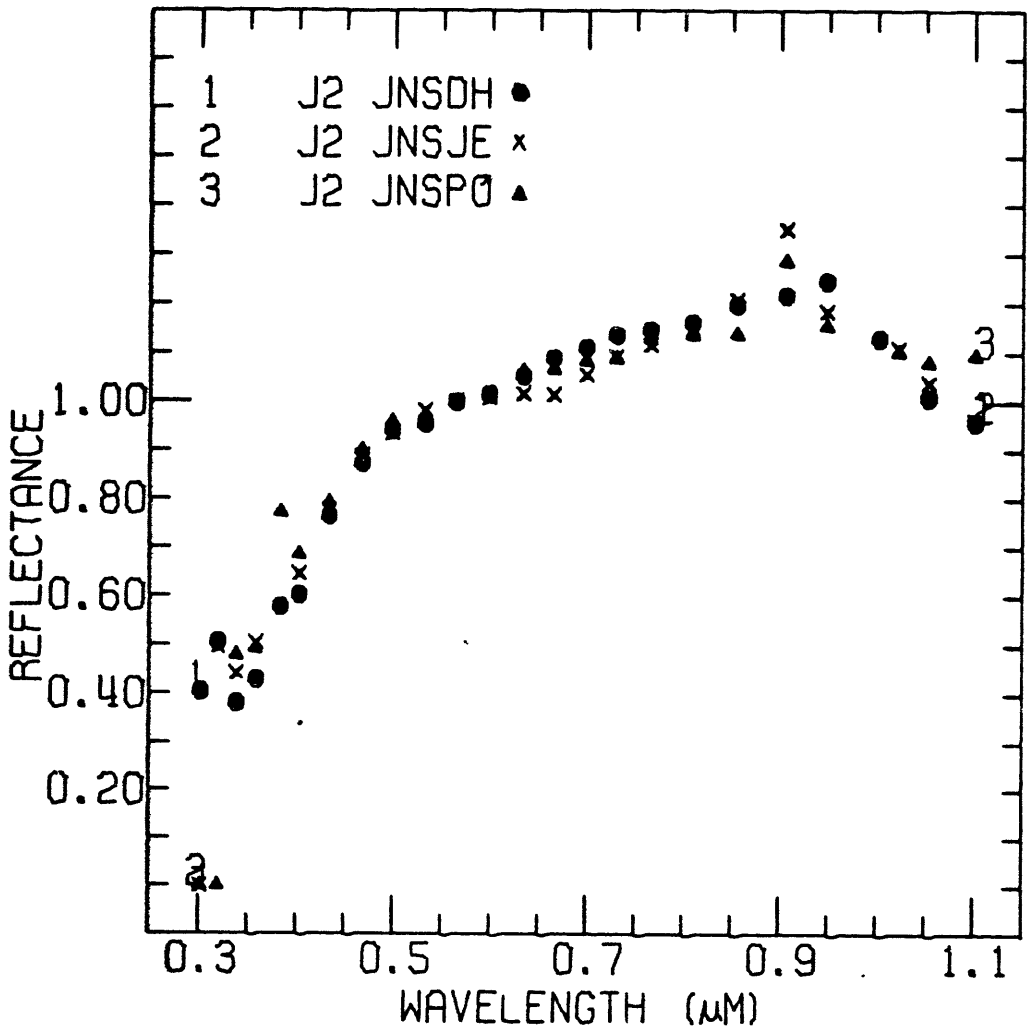

figure 22 b

same as 22 a.

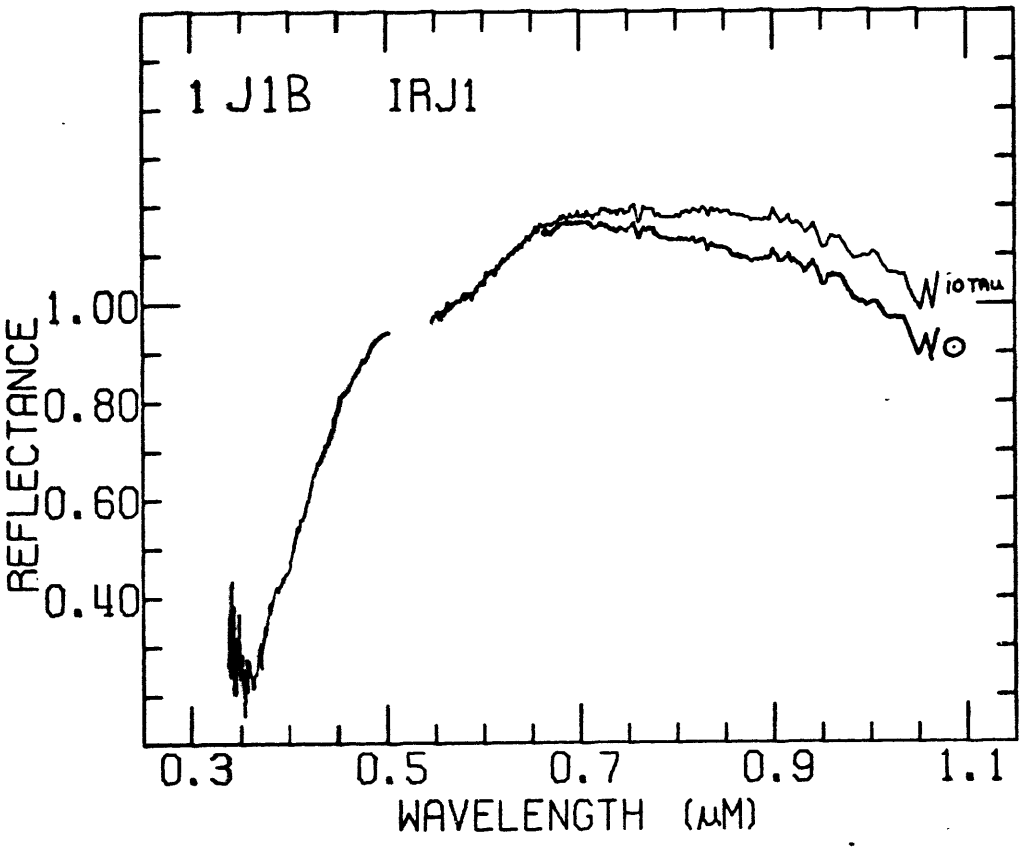

figure 21 a

J1/ 10Tau and J1/ Sun

J3/ 10 Tau and J3/ Sun

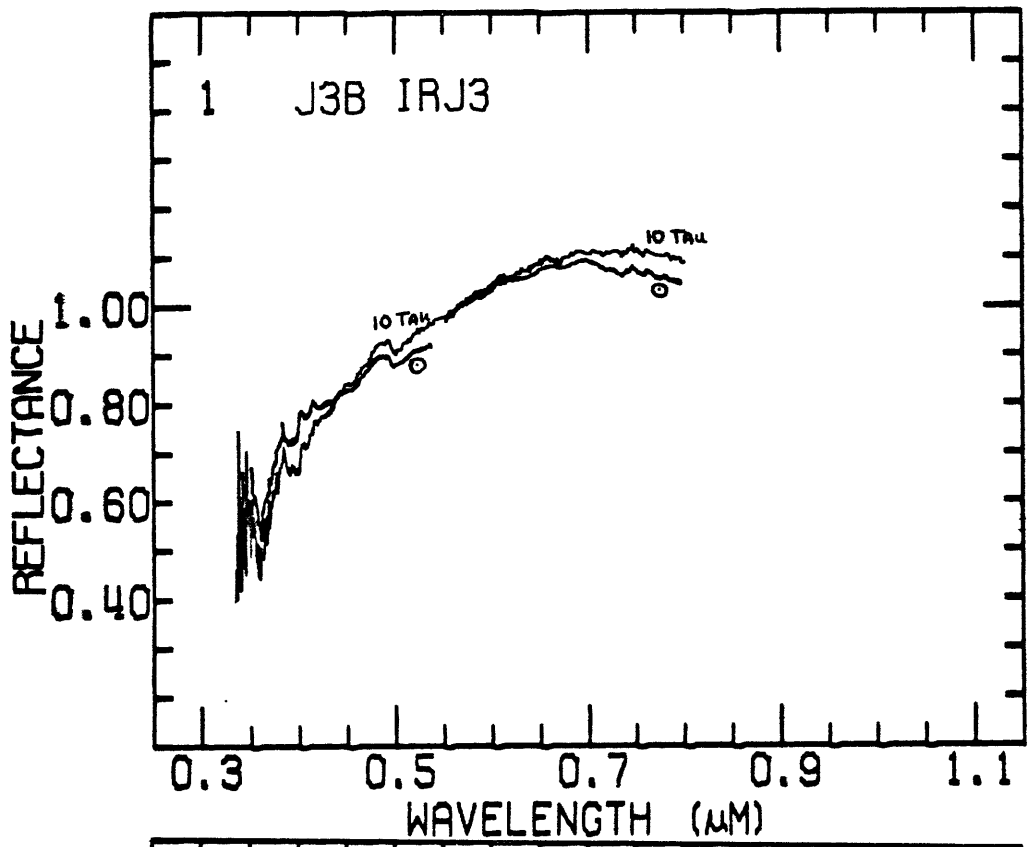

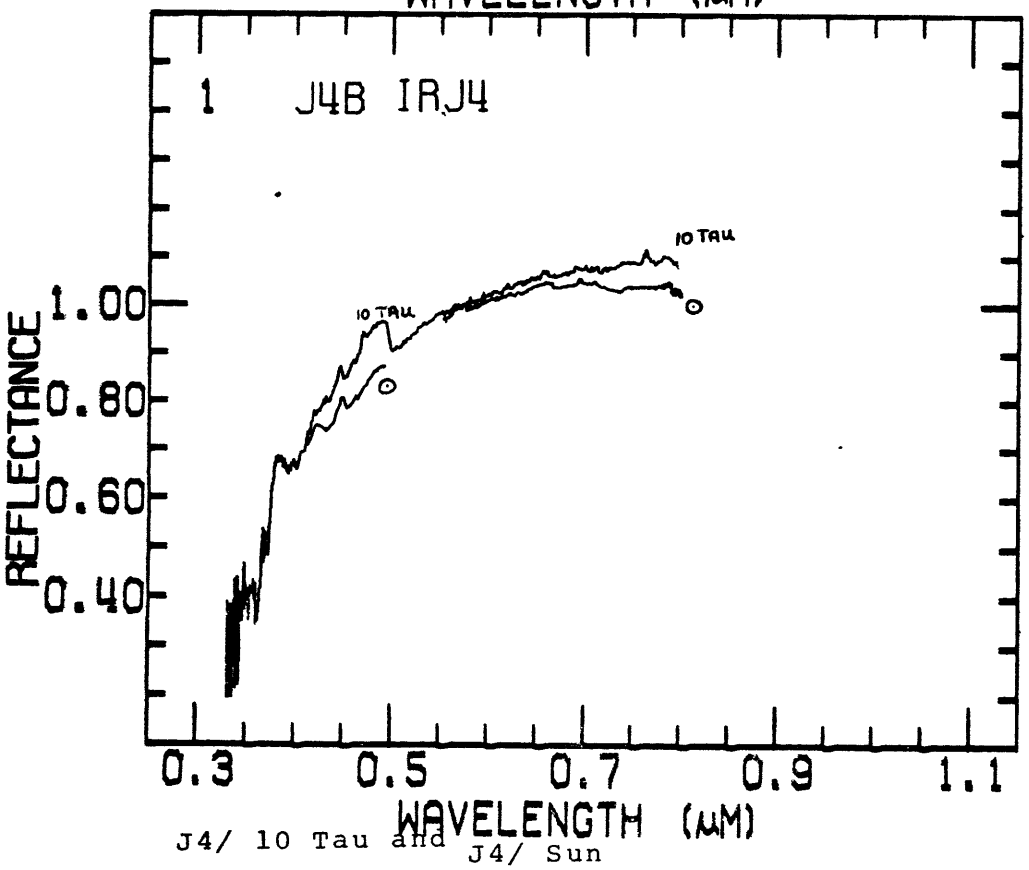

J4/ 10 Tau and J4/ Sun

figure 21 b,c

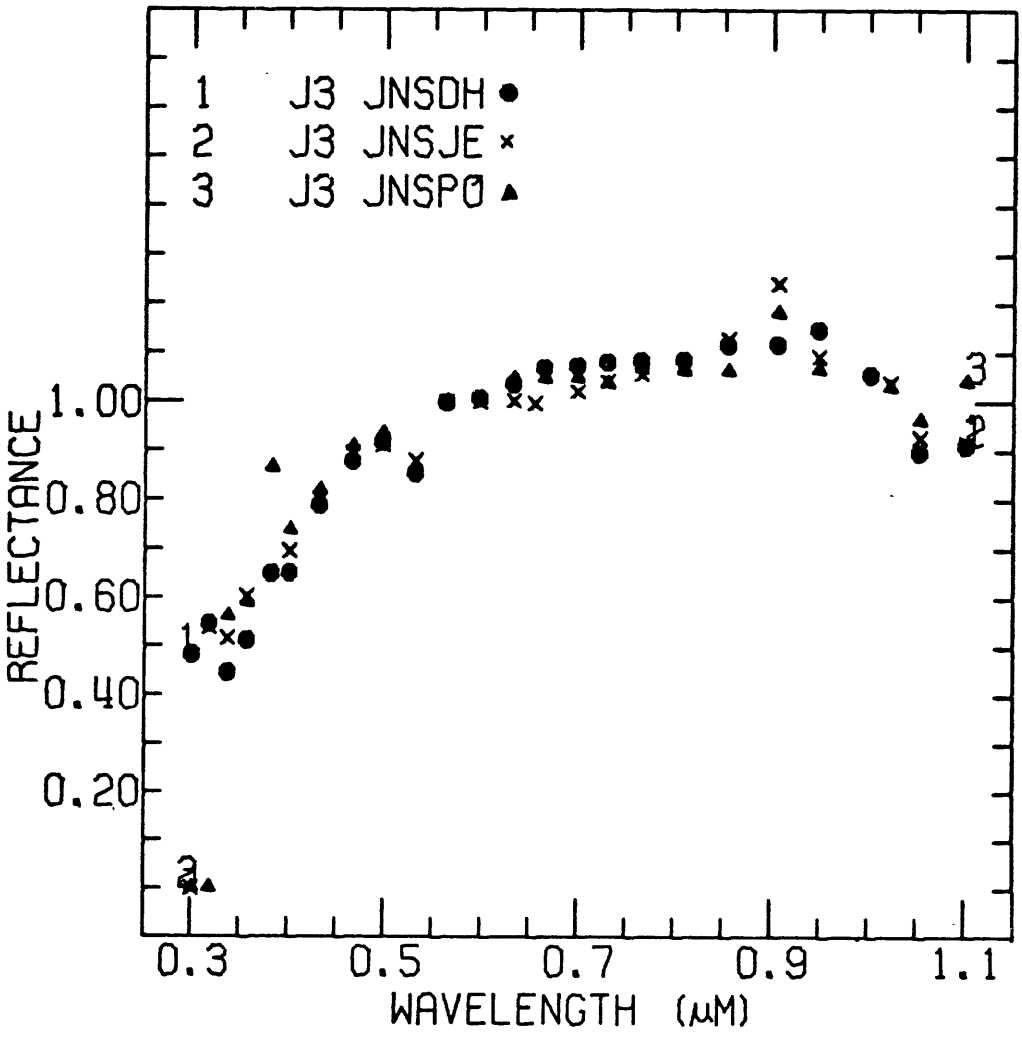

figure 22 c

same as 22 a.

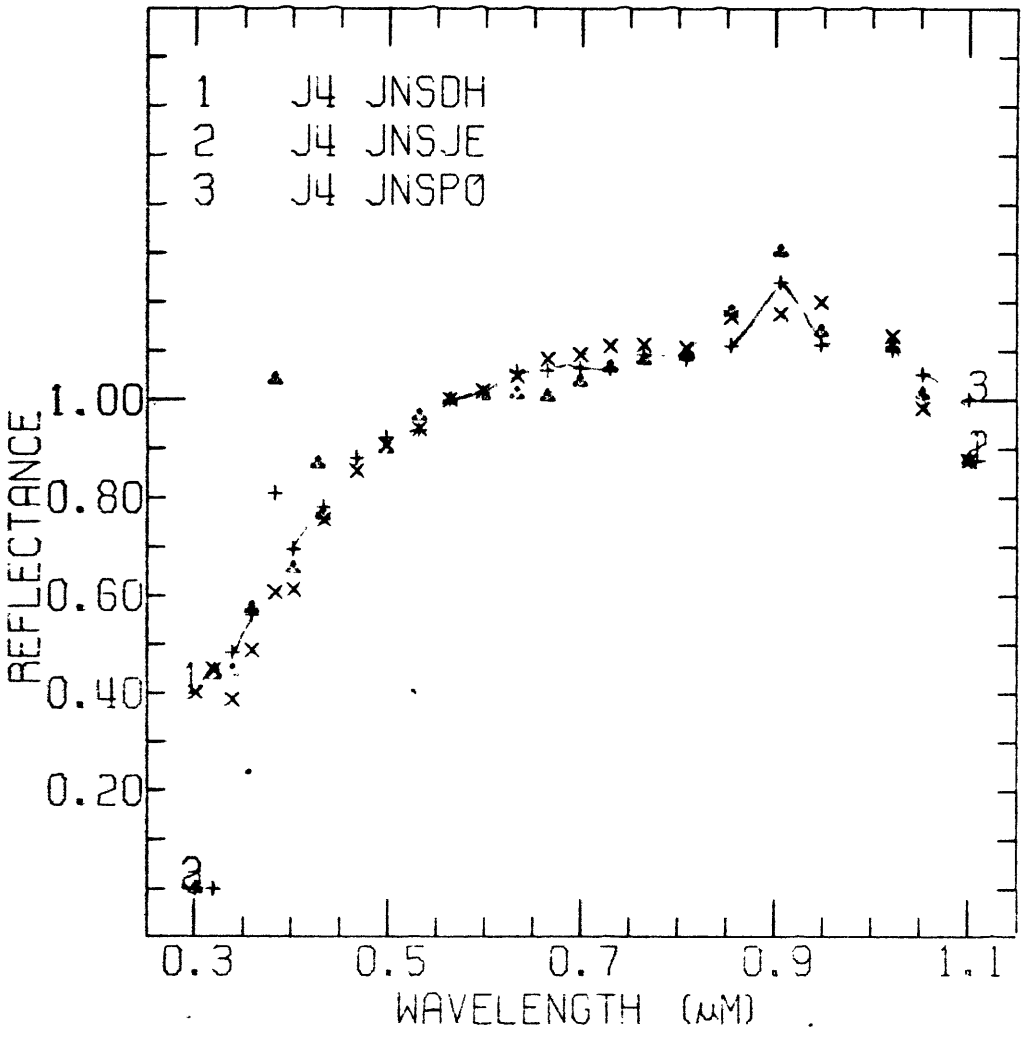

figure 22 d

same as 22 a.

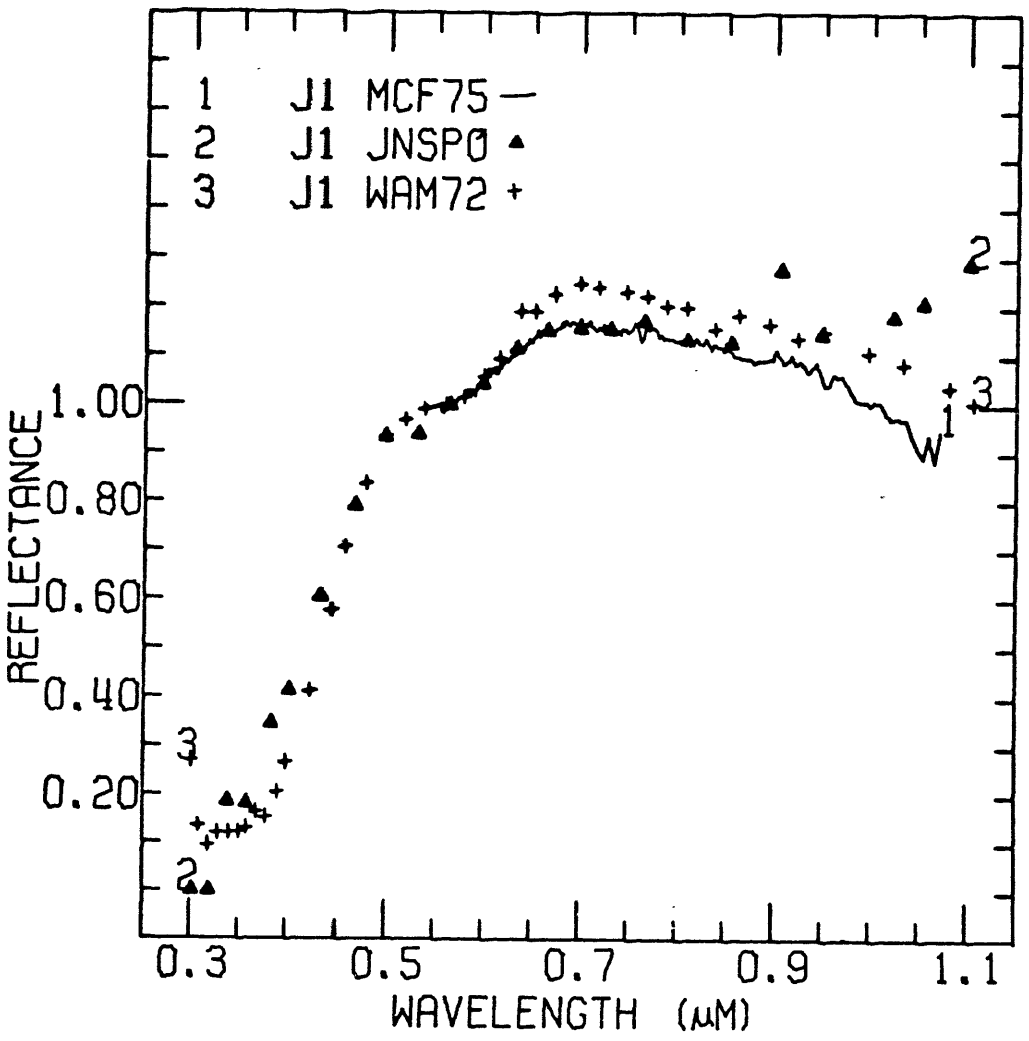

figure 23 a

Three measurements of Io, McFadden, 1975, Johnson, 1970 with star/Sun calibration of Pieters & Owensby et.al. 1977, (JNSPO), and Wamsteker, 1972, (WAM72).

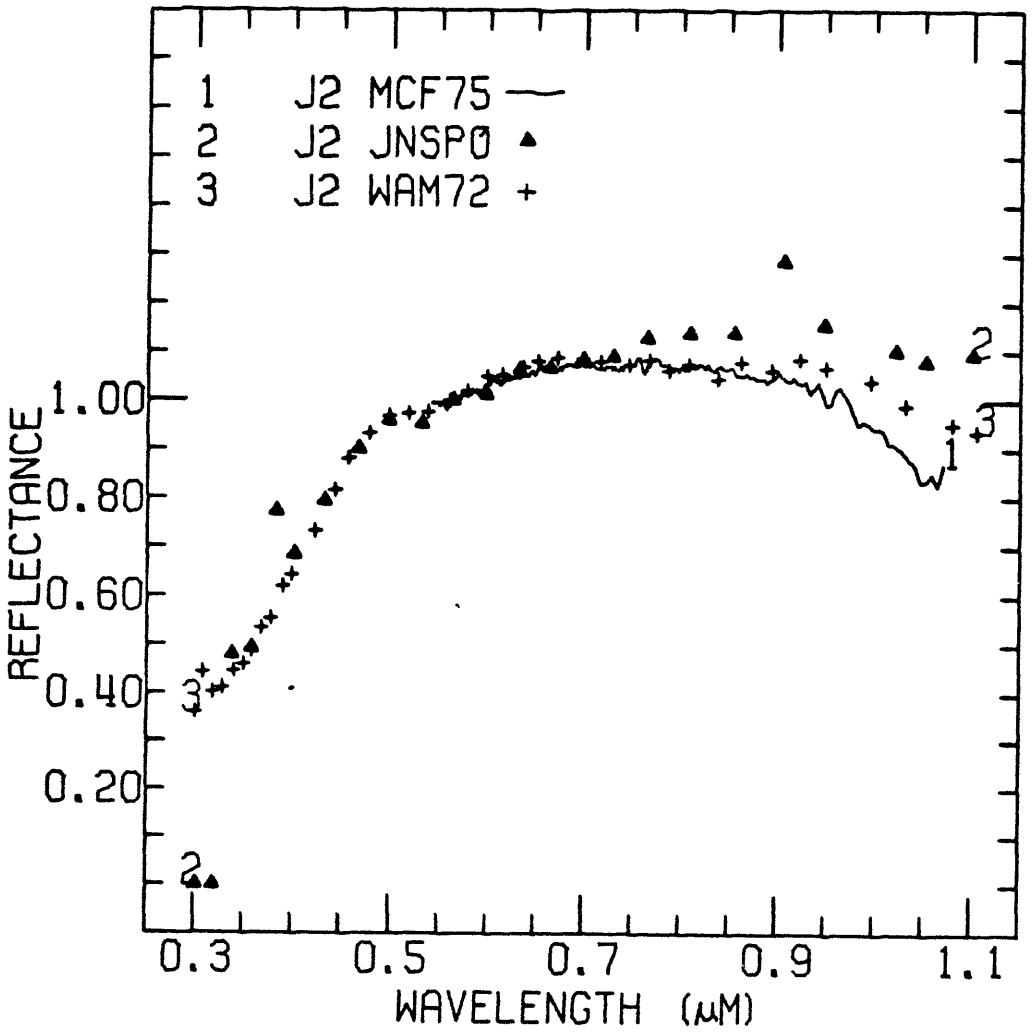

figure 23 b

Galilean satellite, Europa, spectral reflectivity as measured by McFadden, 1975 (MCF75), Johnson, 1970 with star/Sun calibration of Pieter & Owensby et. al., 1977, (JNSPO), and Wamsteker, 1972, (WAM72).

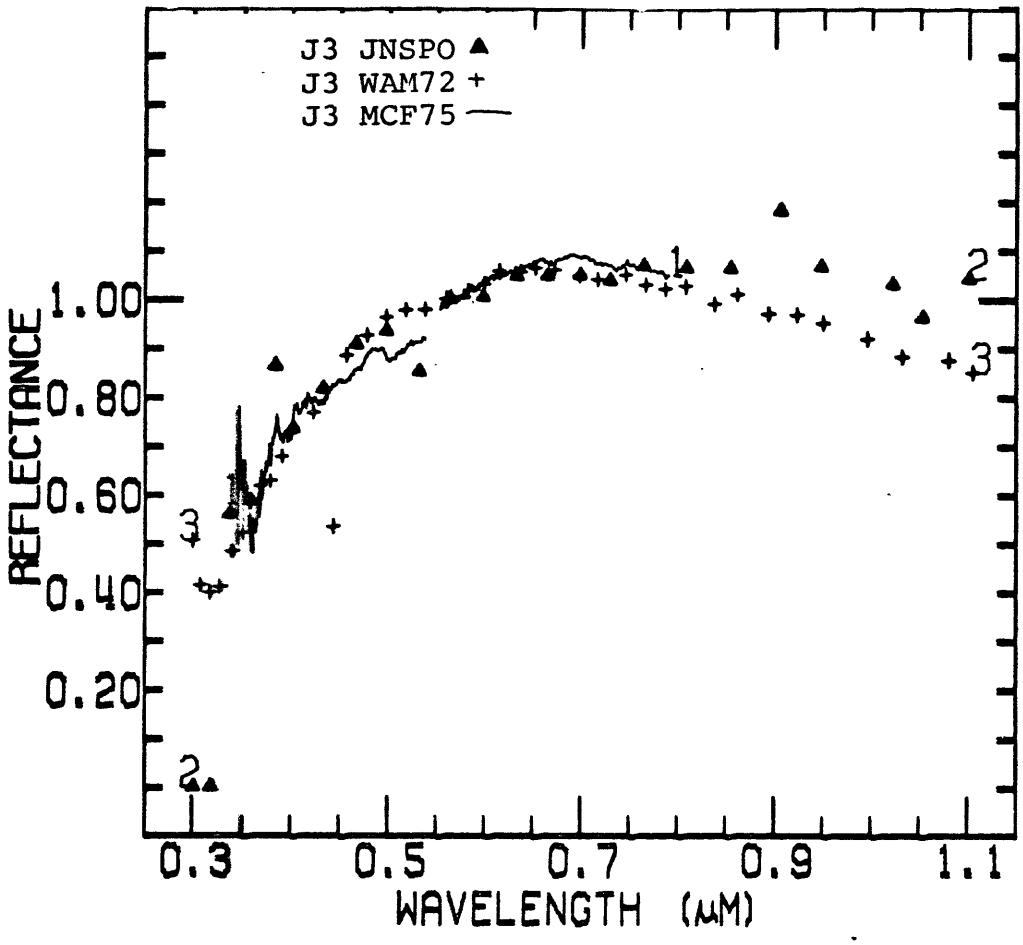

figure 23 c

Galilean satellite, Ganymede, spectral reflectivity, same as 23 a,b.

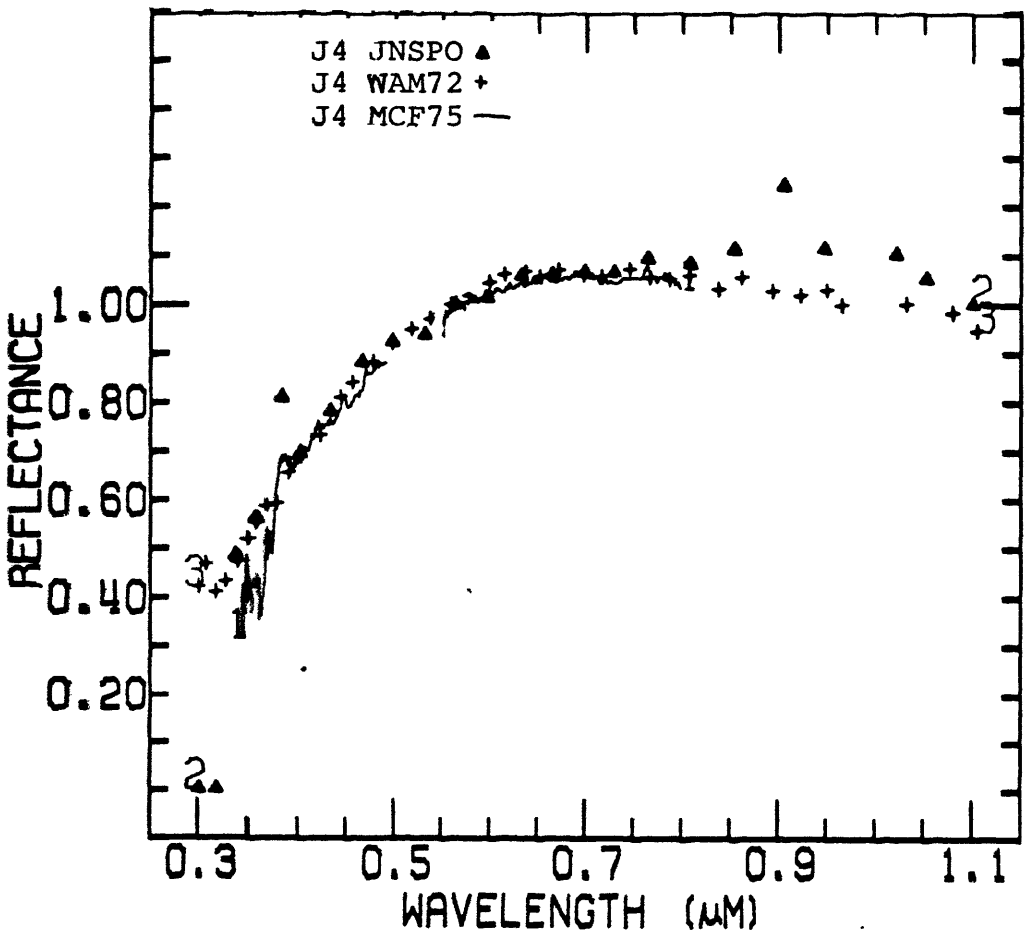

figure 23 d

Galilean satellite, Callisto, spectral reflectivity, same as 23 a,b.

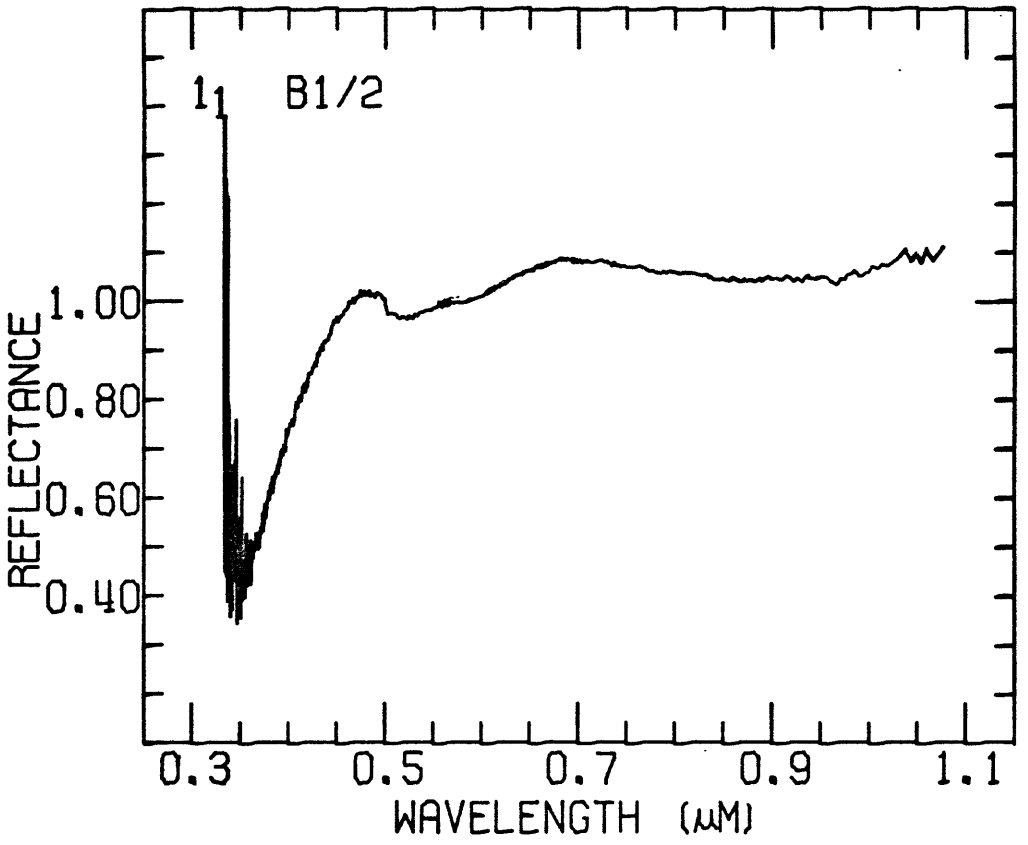

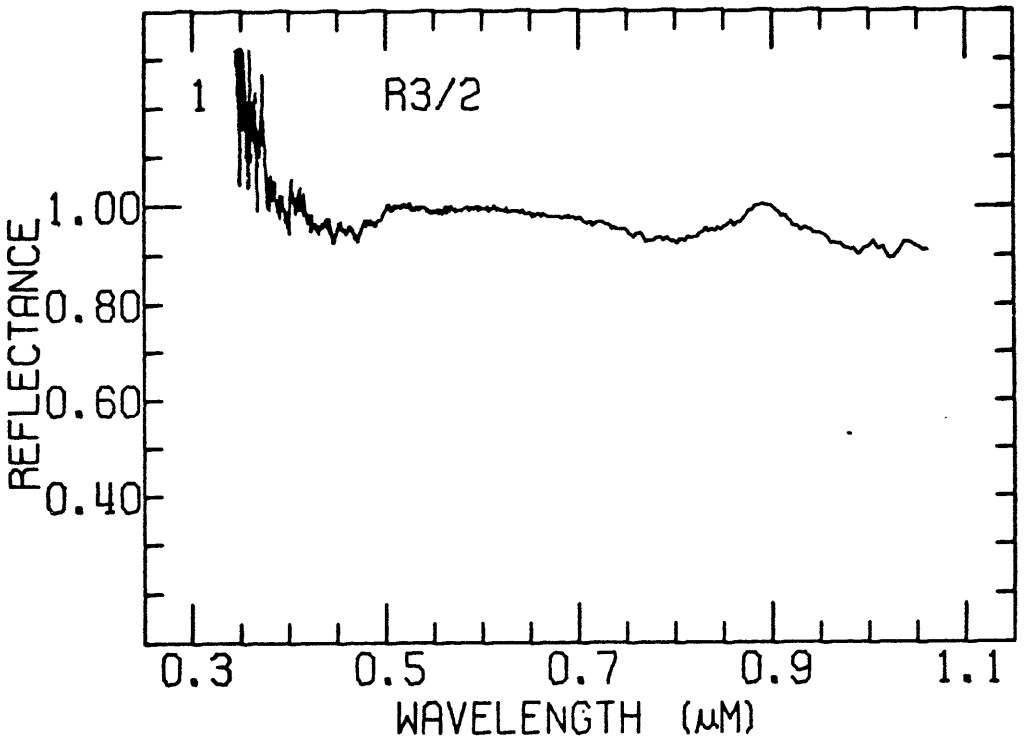

figure 24 a,b

Relative reflectivity of J1/J2 and J3/J2.

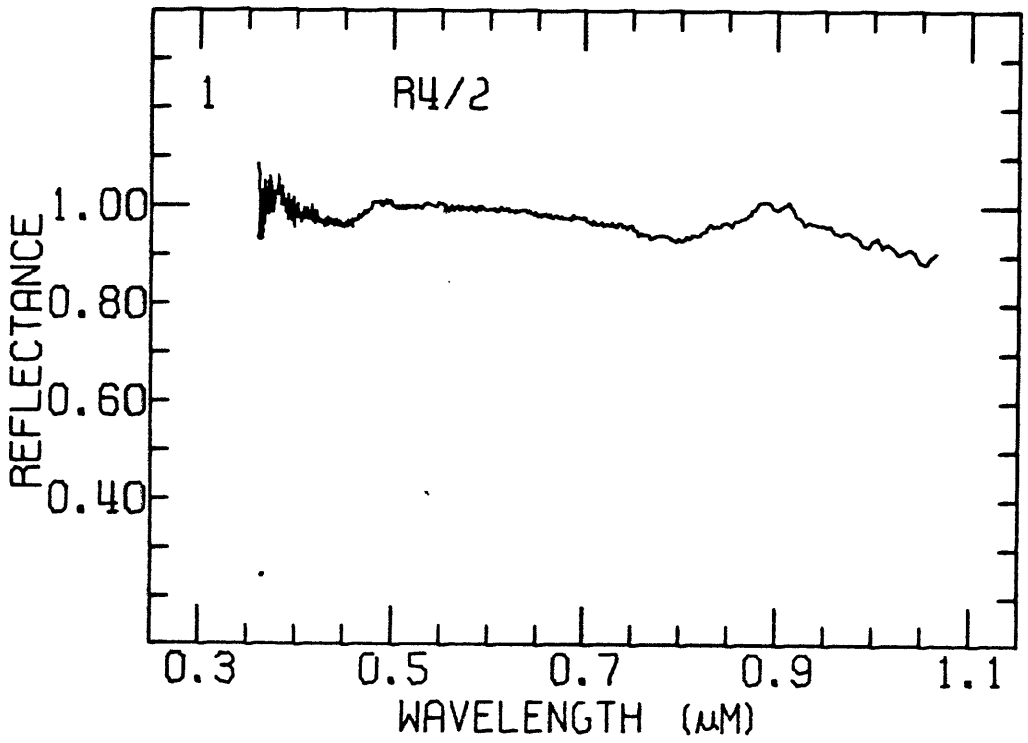

figure 24 c

Relative reflectivity of J4/J2

TABLE 1

from Nash & Fanale (1976)

SPECTRAL FEATURES VS. EXPERIMENTAL VARIABLES FOR EXPLAINING IO LEADING AND TRAILING SIDES DATA. BLOEDITE USED AS TYPICAL NFS COMPONENT

	Occur In Io Spectra		Effect of Experimental Variables														
			Sulfur						NFS Component(s)						Mix		
Spectral Feature	Leading Side	Trailing Side	Hot	Cold	Fine	Coarse	Tight	Loose	Wet	Dry	Fine	Coarse	Natural	Irradiated	High Sulfur	Half & Half	Low Sulfur
Band at ∿ 0.35 μm	O	Δ	•	•	•	•	•	•							•	•	•
Deeper Band		Δ	Δ			Δ		Δ		Δ		Δ		Δ	Δ		
Shallower Band	O			⊖	⊖		⊖		⊖		⊖		⊖				⊖
Minima Shift to Lower λ	O			⊖	⊖		⊖						⊖				⊖
Minima Shift to Higher λ		Δ	Δ			Δ		Δ						Δ	Δ		
Sharp Absorption Edge	O	Δ	•	•	•	•	•	•			⊖				•	•	•
Edge Shift to Lower λ	O			⊖	⊖		⊖						⊖				⊖
Edge Shift to Higher λ		Δ	Δ			Δ		Δ						Δ	Δ	Δ	
Sharper Shoulder	O			⊖	•	•	•	•	⊖		⊖		⊖		⊖		
Rounder Shoulder		Δ	Δ							Δ		Δ		Δ			Δ
Inflection at 0.5 μm		Δ												Δ	•	•	•

Explanation:

- Dot (•) indicates that spectral feature is affected favorably by this experimental variable.
- Symbols O and Δ indicate this spectral feature present in Io spectra of leading and trailing sides, respectively.
- Combined dot and symbol indicates experimental variable that may contribute to causing spectral feature in Io spectra.

Table 2

Satellite	prism	orbital phase	air mass	air mass 10 Tau
Io	blue	25.5^{o}- 26.0^{o}	1.06	1.07
Io	IR	28.0^{o}-28.4^{o}	1.08	1.06
Europa	blue	2.2^{o}	1.06	1.07
Europa	IR	2.2^{o}	1.08	1.06
Ganymede	blue	58.8^{o}	1.20	1.20
Ganymede	IR	59.0^{o}	1.20	1.18
Callisto	blue	99.4^{o}	1.27-1.28	1.30
Callisto	IR	99.2^{o}	1.22-1.24	1.24

Table 3 a- Io/ Sun

JB	0.3282	0.0	0.3286	40.554	0.3291	1.806	0.3295	2.819
	0.3300	-3.66C	C.33C4	-0.734	0.3309	2.725	0.3313	1.368
	0.3318	2.766	C.3322	0.899	0.3327	2.443	0.3332	0.C42
	0.3336	0.92C	0.3341	0.530	0.3346	0.429	0.3350	0.142
	0.3355	0.278	C.3360	C.226	0.3365	C.199	0.3370	0.440
	0.3374	0.173	0.3379	0.258	0.3384	0.263	0.3389	0.319
	0.3394	0.180	C.3399	C.194	0.3404	0.198	0.3409	0.285
	0.3414	0.2C2	C.3419	C.155	C.3424	0.211	0.3429	0.230
	0.3435	0.198	C.3440	0.188	C.3445	0.229	0.3450	C.271
	C.3456	0.178	C.3461	C.275	0.3466	0.254	0.3472	0.158
	0.3477	0.250	0.3482	0.179	0.3488	C.223	0.3493	0.211
	0.3499	0.2C8	C.3504	C.207	0.351C	C.130	0.3516	0.219
	0.3521	C.191	0.3527	0.160	0.3533	0.197	0.3538	0.181
	0.3544	0.147	0.3550	0.211	0.3556	0.161	0.3562	0.202
	0.3567	0.195	0.3573	C.21C	0.3579	C.193	0.3585	C.2CC
	0.3591	0.164	0.3597	C.177	0.3604	0.191	0.3610	0.178
	0.3616	0.172	0.3622	C.160	0.3628	0.186	0.3635	0.187
	0.3641	0.179	0.3647	0.191	0.3654	0.213	0.3660	0.227
	0.3667	0.192	0.3673	C.231	0.368C	C.239	0.3686	0.239
	0.3693	0.2CC	0.3699	0.232	0.37C6	0.23C	0.3713	0.246
	0.3720	0.253	0.3727	0.234	0.3733	0.266	0.3740	0.264
	0.3747	0.263	0.3754	0.251	0.3761	0.273	0.3768	0.272
	0.3776	0.299	C.3783	0.288	0.3790	0.287	0.3797	0.296
	0.3805	0.29C	0.3812	C.302	0.3819	0.302	0.3827	0.315
	0.3834	0.314	0.3842	0.319	0.3849	0.325	0.3857	0.331
	0.3865	0.327	0.3873	C.330	0.388C	C.336	0.3888	0.340
	0.3896	0.332	C.39C4	0.342	0.3912	C.352	0.392C	C.343
	C.3928	0.345	C.3936	C.359	0.3945	0.360	0.3953	0.362
	0.3961	0.356	0.397C	C.362	0.3978	C.381	C.3987	C.373
	0.3995	0.377	0.4004	0.380	0.4012	0.391	0.4021	0.390
	0.4030	0.392	0.4C39	C.403	0.4048	0.417	0.4057	0.421
	0.4066	0.420	0.4C75	C.433	0.4C84	0.428	0.4093	0.425
	0.4103	0.431	0.4112	C.430	0.4122	0.438	0.4131	0.449
	0.4141	0.446	0.4150	C.452	0.4160	0.460	0.4170	0.458
	0.4180	0.465	C.4190	0.466	C.4200	0.475	0.4210	0.478
	0.4220	0.483	0.4230	0.492	0.4241	0.487	0.4251	0.498
	0.4261	0.497	0.4272	C.500	0.4283	0.505	0.4293	0.505
	0.4304	0.505	0.4315	0.512	0.4326	0.518	0.4337	0.517
	0.4348	0.525	0.4359	0.524	0.4371	0.530	0.4382	0.529
	0.4394	0.541	C.44C5	C.544	0.4417	C.552	0.4429	0.552
	0.4441	0.566	0.4453	0.566	0.4465	0.576	0.4477	C.577
	0.4489	0.587	C.4501	C.597	0.4514	0.587	0.4527	0.589
	0.4539	0.599	0.4552	C.594	0.4565	C.6C2	0.4578	0.599
	0.4591	0.6C9	0.4604	C.387	0.4618	C.39C	0.4631	0.391
	0.4645	0.395	0.4658	C.396	0.4672	0.399	0.4686	0.397
	0.4700	0.4C2	0.4714	C.407	0.4729	C.4C5	0.4743	C.404
	0.4758	0.402	0.4772	0.408	0.4787	0.411	0.4802	0.412
	0.4817	0.419	0.4832	C.419	0.4848	0.418	0.4863	0.425

Table 3a cont. Io/ Sun

	0.4879	0.423	0.4895	0.425	0.4911	0.427	0.4927	0.425
	0.4943	0.425	0.4959	0.428	0.4976	0.426	0.4993	0.428
	0.5010	0.429	0.5027	0.438	0.5044	0.452	0.5061	0.466
	0.5079	0.481	0.5097	0.497	0.5114	0.504	0.5132	0.526
	0.5151	0.540	0.5169	0.551	0.5188	0.578	0.5207	0.590
	0.5226	0.608	0.5245	0.628	0.5264	0.649	0.5284	0.666
	0.5304	0.692	0.5324	0.709	0.5344	0.731	0.5364	0.752
	0.5385	0.775	0.5406	0.801	0.5427	0.821	0.5448	0.850
IRJ1	0.5455	0.867	0.5464	0.919	0.5473	0.975	0.5482	0.982
IRJ1	0.5491	0.987	0.5500	0.988	0.5509	0.986	0.5518	0.987
IRJ1	0.5527	0.992	0.5536	0.987	0.5546	0.990	0.5555	0.977
IRJ1	0.5564	0.989	0.5574	0.975	0.5583	0.992	0.5593	0.992
IRJ1	0.5602	0.990	0.5612	0.983	0.5622	0.994	0.5632	0.991
IRJ1	0.5641	1.006	0.5651	0.987	0.5661	0.992	0.5671	0.999
IRJ1	0.5681	0.994	0.5691	0.994	0.5702	0.997	0.5712	1.003
IRJ1	0.5722	1.001	0.5732	1.006	0.5743	1.007	0.5753	1.005
IRJ1	0.5764	1.006	0.5774	1.002	0.5785	1.013	0.5796	1.011
IRJ1	0.5807	1.018	0.5817	1.021	0.5828	1.009	0.5839	1.022
IRJ1	0.5850	1.016	0.5862	1.014	0.5873	1.019	0.5884	1.021
IRJ1	0.5895	1.008	0.5907	1.022	0.5918	1.027	0.5930	1.029
IRJ1	0.5941	1.026	0.5953	1.034	0.5965	1.035	0.5977	1.043
IRJ1	0.5989	1.039	0.6001	1.042	0.6013	1.046	0.6025	1.042
IRJ1	0.6037	1.064	0.6049	1.057	0.6062	1.059	0.6074	1.062
IRJ1	0.6087	1.059	0.6099	1.065	0.6112	1.067	0.6125	1.056
IRJ1	0.6138	1.056	0.6151	1.073	0.6164	1.071	0.6177	1.066
IRJ1	0.6190	1.079	0.6204	1.075	0.6217	1.085	0.6230	1.081
IRJ1	0.6244	1.083	0.6258	1.084	0.6272	1.091	0.6285	1.089
IRJ1	0.6299	1.094	0.6313	1.098	0.6328	1.093	0.6342	1.102
IRJ1	0.6356	1.104	0.6371	1.098	0.6385	1.107	0.6400	1.110
IRJ1	0.6415	1.104	0.6430	1.114	0.6445	1.116	0.6460	1.123
IRJ1	0.6475	1.122	0.6490	1.116	0.6506	1.124	0.6521	1.128
IRJ1	0.6537	1.133	0.6552	1.142	0.6568	1.130	0.6584	1.141
IRJ1	0.6600	1.146	0.6617	1.142	0.6633	1.143	0.6649	1.139
IRJ1	0.6666	1.145	0.6683	1.142	0.6700	1.144	0.6717	1.141
IRJ1	0.6734	1.146	0.6751	1.149	0.6768	1.149	0.6786	1.151
IRJ1	0.6803	1.159	0.6821	1.154	0.6839	1.160	0.6857	1.158
IRJ1	0.6875	1.153	0.6894	1.158	0.6912	1.163	0.6931	1.156
IRJ1	0.6950	1.157	0.6969	1.158	0.6988	1.168	0.7007	1.155
IRJ1	0.7026	1.154	0.7046	1.158	0.7065	1.152	0.7085	1.162
IRJ1	0.7105	1.153	0.7126	1.143	0.7146	1.142	0.7166	1.146
IRJ1	0.7187	1.150	0.7208	1.145	0.7229	1.154	0.7250	1.152
IRJ1	0.7272	1.153	0.7293	1.144	0.7315	1.146	0.7337	1.138
IRJ1	0.7359	1.140	0.7382	1.145	0.7404	1.135	0.7427	1.146
IRJ1	0.7450	1.147	0.7473	1.140	0.7497	1.141	0.7520	1.144
IRJ1	0.7544	1.157	0.7568	1.158	0.7592	1.143	0.7617	1.122
IRJ1	0.7641	1.128	0.7666	1.154	0.7691	1.149	0.7717	1.147
IRJ1	0.7742	1.148	0.7768	1.145	0.7794	1.129	0.7821	1.133
IRJ1	0.7847	1.129	0.7874	1.125	0.7901	1.125	0.7928	1.124
IRJ1	0.7956	1.122	0.7984	1.119	0.8012	1.124	0.8040	1.118

Table 3a cont. Io/ Sun

IRJ1	0.8069	1.126	0.8098	1.126	0.8127	1.123	0.8157	1.120
IRJ1	0.8187	1.127	0.8217	1.121	0.8248	1.115	0.8278	1.127
IRJ1	0.8310	1.119	0.8341	1.104	0.8373	1.118	0.8405	1.111
IRJ1	0.8437	1.110	0.8470	1.103	0.8503	1.104	0.8537	1.104
IRJ1	0.8571	1.094	0.8605	1.092	0.8639	1.088	0.8674	1.089
IRJ1	0.8710	1.085	0.8745	1.085	0.8782	1.079	0.8818	1.081
IRJ1	0.8855	1.083	0.8892	1.081	0.8930	1.086	0.8968	1.084
IRJ1	0.9007	1.106	0.9046	1.091	0.9086	1.078	0.9126	1.083
IRJ1	0.9166	1.094	0.9207	1.075	0.9249	1.081	0.9290	1.076
IRJ1	0.9333	1.058	0.9376	1.066	0.9419	1.080	0.9463	1.057
IRJ1	0.9508	1.033	0.9553	1.035	0.9599	1.055	0.9645	1.052
IRJ1	0.9692	1.053	0.9739	1.036	0.9787	1.017	0.9836	1.001
IRJ1	0.9885	0.998	0.9935	0.999	0.9986	0.992	1.0037	1.000
IRJ1	1.0089	0.997	1.0141	0.976	1.0195	0.965	1.0249	0.967
IRJ1	1.0304	0.963	1.0359	0.962	1.0416	0.928	1.0473	0.902
IRJ1	1.0531	0.884	1.0589	0.931	1.0649	0.876	1.0709	0.939

Table 3b Europa/ Sun

ELRB	0.3355	0.352	C.3360	C.284	0.3365	0.391	0.3370	0.4CC
ELRB	0.3374	0.457	C.3379	C.320	0.3384	0.354	0.3389	0.464
EURB	0.3394	0.33C	C.3399	0.454	C.34C4	C.5C7	0.3409	0.474
ELRB	0.3414	0.326	0.3419	C.406	0.3424	C.524	C.3429	C.4C6
EURB	0.3435	0.444	C.3440	0.438	0.3445	0.427	0.3450	0.415
EURB	0.3456	0.4CC	0.3461	C.380	0.3466	0.487	0.3472	0.465
EURB	0.3477	0.492	0.3482	C.421	0.3488	C.392	C.3493	0.447
EURB	C.3499	0.466	0.3504	0.420	0.3510	0.370	0.3516	0.469
EURB	0.3521	0.319	C.3527	C.413	0.3533	0.429	0.3538	0.390
EURB	0.3544	0.346	0.3550	0.474	C.3556	C.398	0.3562	0.386
ELRB	0.3567	0.443	0.3573	0.411	0.3579	0.451	0.3585	0.404
EURB	0.3591	0.374	C.3597	C.374	C.3604	0.397	0.3610	0.358
EURB	0.3616	0.41C	0.3622	C.364	0.3628	0.372	0.3635	0.368
ELRB	0.3641	0.373	0.3647	0.388	0.3654	0.428	0.3660	C.428
EURB	0.3667	0.385	C.3673	C.446	0.3680	0.451	0.3686	0.457
EURB	0.3693	0.4C9	C.3699	C.454	0.37C6	C.461	0.3713	0.456
EURB	0.3720	0.476	0.3727	C.445	C.3733	C.470	0.3740	0.460
EURB	0.3747	0.487	0.3754	0.427	0.3761	0.477	0.3768	0.486
EURB	0.3776	0.522	0.3783	0.488	0.3790	0.473	0.3797	0.485
EURB	0.3805	0.483	0.3812	C.484	0.3819	0.482	0.3827	C.499
EURB	0.3834	0.495	0.3842	0.520	0.3849	0.513	0.3857	0.520
EURB	0.3865	0.506	0.3873	C.510	0.3880	C.513	0.3888	0.512
EURB	0.3896	0.508	C.3904	C.504	C.3912	C.523	C.3920	0.497
ELRB	0.3928	0.504	0.3936	0.513	0.3945	0.523	0.3953	0.509
EURB	0.3961	0.507	C.3970	C.514	0.3978	0.517	0.3987	0.516
EURB	0.3995	0.518	C.4CC4	0.515	C.4012	C.525	C.4021	0.521
ELRB	0.4030	0.526	0.4039	0.536	0.4048	0.551	0.4057	0.561
ELRB	0.4066	0.555	C.4C75	C.552	0.4084	C.540	0.4093	0.542
EURB	0.4103	0.548	C.4112	C.54C	C.4122	C.545	0.4131	0.562
EURB	0.4141	0.555	0.4150	C.550	C.416C	C.563	0.4170	0.554
EURB	0.418C	0.568	0.4190	0.558	C.4200	0.573	0.4210	0.563
EURB	0.4220	0.569	0.4230	0.576	C.4241	0.572	0.4251	0.577
EURB	0.4261	0.576	0.4272	0.575	0.4283	0.579	0.4293	0.579
EURB	0.4304	0.566	0.4315	C.575	0.4326	0.578	0.4337	0.573
EURB	0.4348	0.578	0.4359	C.580	0.4371	0.577	0.4382	0.578
ELRB	0.4394	0.589	0.4405	C.591	C.4417	C.597	0.4429	0.592
EURB	0.4441	0.605	0.4453	C.597	0.4465	0.603	0.4477	0.601
EURB	0.4489	0.612	C.45C1	C.619	0.4514	C.614	0.4527	0.611
ELRB	0.4539	0.619	0.4552	C.613	0.4565	C.618	0.4578	C.614
EURB	0.4591	0.620	C.46C4	C.393	0.4618	C.393	0.4631	0.392
EURB	0.4645	C.397	0.4658	C.396	0.4672	C.398	0.4686	0.398
EURB	0.4700	0.4CC	0.4714	C.402	0.4729	C.4CC	C.4743	C.397
EURB	0.4758	0.398	0.4772	0.402	0.4787	0.404	0.4802	0.407
EURB	0.4817	0.413	C.4832	C.412	0.4848	0.414	0.4863	0.419
EURB	0.4879	0.419	C.4895	C.422	0.4911	C.422	C.4927	C.419

Table 3b cont. Europa/ Sun

EURB		0.4943	0.420	0.4959	0.424	0.4976	0.425	0.4993	0.428
EURB		0.5010	0.437	0.5027	0.451	0.5044	0.464	0.5061	0.479
EURB		0.5079	0.494	0.5097	0.511	0.5114	0.520	0.5132	0.545
EURB		0.5151	0.560	0.5169	0.571	0.5188	0.598	0.5207	0.613
EURB		0.5226	0.632	0.5245	0.651	0.5264	0.672	0.5284	0.690
EURB		0.5304	0.714	0.5324	0.732	0.5344	0.752	0.5364	0.772
EURB		0.5385	0.794	0.5406	0.817	0.5427	0.839	0.5448	0.865
EI	IRJ2	0.5455	0.838	0.5464	0.900	0.5473	0.968	0.5482	0.981
EI	IRJ2	0.5491	0.990	0.5500	0.984	0.5509	0.987	0.5518	0.987
EI	IRJ2	0.5527	0.990	0.5536	0.989	0.5546	0.992	0.5555	0.979
EI	IRJ2	0.5564	0.988	0.5574	0.975	0.5583	0.995	0.5593	0.996
	IRJ2	0.5602	0.992	0.5612	0.985	0.5622	0.993	0.5632	0.996
	IRJ2	0.5641	1.005	0.5651	0.990	0.5661	0.995	0.5671	0.998
	IRJ2	0.5681	0.993	0.5691	0.996	0.5702	0.998	0.5712	1.005
	IRJ2	0.5722	0.998	0.5732	1.008	0.5743	1.005	0.5753	1.004
	IRJ2	0.5764	1.004	0.5774	1.001	0.5785	1.011	0.5796	1.009
	IRJ2	0.5807	1.015	0.5817	1.015	0.5828	1.007	0.5839	1.016
	IRJ2	0.5850	1.012	0.5862	1.011	0.5873	1.016	0.5884	1.013
	IRJ2	0.5895	1.003	0.5907	1.014	0.5918	1.016	0.5930	1.015
	IRJ2	0.5941	1.015	0.5953	1.021	0.5965	1.027	0.5977	1.029
	IRJ2	0.5989	1.026	0.6001	1.025	0.6013	1.029	0.6025	1.026
	IRJ2	0.6037	1.043	0.6049	1.038	0.6062	1.034	0.6074	1.041
	IRJ2	0.6087	1.032	0.6099	1.039	0.6112	1.039	0.6125	1.026
	IRJ2	0.6138	1.024	0.6151	1.038	0.6164	1.037	0.6177	1.032
	IRJ2	0.6190	1.041	0.6204	1.036	0.6217	1.044	0.6230	1.038
	IRJ2	0.6244	1.041	0.6258	1.039	0.6272	1.043	0.6285	1.041
	IRJ2	0.6299	1.044	0.6313	1.046	0.6328	1.041	0.6342	1.047
	IRJ2	0.6356	1.046	0.6371	1.044	0.6385	1.045	0.6400	1.049
	IRJ2	0.6415	1.044	0.6430	1.048	0.6445	1.052	0.6460	1.057
	IRJ2	0.6475	1.054	0.6490	1.046	0.6506	1.050	0.6521	1.060
	IRJ2	0.6537	1.060	0.6552	1.067	0.6568	1.058	0.6584	1.062
	IRJ2	0.6600	1.067	0.6617	1.065	0.6633	1.060	0.6649	1.058
	IRJ2	0.6666	1.065	0.6683	1.059	0.6700	1.059	0.6717	1.054
	IRJ2	0.6734	1.058	0.6751	1.063	0.6768	1.058	0.6786	1.063
	IRJ2	0.6803	1.068	0.6821	1.066	0.6839	1.069	0.6857	1.067
	IRJ2	0.6875	1.067	0.6894	1.063	0.6912	1.072	0.6931	1.064
	IRJ2	0.6950	1.066	0.6969	1.070	0.6988	1.077	0.7007	1.063
	IRJ2	0.7026	1.065	0.7046	1.069	0.7065	1.064	0.7085	1.072
	IRJ2	0.7105	1.067	0.7126	1.059	0.7146	1.058	0.7166	1.059
	IRJ2	0.7187	1.062	0.7208	1.058	0.7229	1.066	0.7250	1.064
	IRJ2	0.7272	1.066	0.7293	1.058	0.7315	1.063	0.7337	1.059
	IRJ2	0.7359	1.056	0.7382	1.065	0.7404	1.058	0.7427	1.069
	IRJ2	0.7450	1.070	0.7473	1.067	0.7497	1.069	0.7520	1.071
	IRJ2	0.7544	1.083	0.7568	1.084	0.7592	1.070	0.7617	1.049
	IRJ2	0.7641	1.057	0.7666	1.077	0.7691	1.078	0.7717	1.082
	IRJ2	0.7742	1.080	0.7768	1.078	0.7794	1.068	0.7821	1.068
	IRJ2	0.7847	1.067	0.7874	1.063	0.7901	1.061	0.7928	1.059
	IRJ2	0.7956	1.061	0.7984	1.054	0.8012	1.063	0.8040	1.057

Table 3b cont. Europa/ Sun

IRJ2	0.8069	1.063	0.8098	1.066	C.8127	1.C61	C.8157	1.C62
IRJ2	0.8187	1.068	0.8217	1.068	0.8248	1.060	0.8278	1.070
IRJ2	0.8310	1.C58	C.8341	1.C53	0.8373	1.062	C.8405	1.066
IRJ2	0.8437	1.06C	0.8470	1.057	C.85C3	1.C60	0.8537	1.063
IRJ2	0.8571	1.C44	C.8605	1.C46	C.8639	1.C45	0.8674	1.C49
IRJ2	0.8710	1.043	C.8745	1.C42	0.8782	1.C39	0.8818	1.037
IRJ2	0.8855	1.041	C.8892	1.C31	C.8930	1.C36	0.8968	1.041
IRJ2	0.9C07	1.053	0.9046	1.045	0.9086	1.035	0.9126	1.032
IRJ2	0.9166	1.043	0.9207	1.C31	0.9249	1.028	0.9290	1.033
IRJ2	0.9333	1.C09	C.9376	1.C19	C.9419	1.C32	0.9463	1.007
IRJ2	0.9508	0.984	0.9553	0.988	C.9599	1.016	0.9645	1.021
IRJ2	0.9692	1.006	0.9739	C.990	0.9787	C.966	0.9836	0.944
IRJ2	0.9885	0.952	C.9935	C.948	0.9986	C.938	1.C037	0.935
IRJ2	1.C089	0.934	1.0141	C.906	1.C195	C.9C5	1.C249	0.896
IRJ2	1.C304	0.888	1.0359	0.872	1.0416	0.864	1.0473	0.829
IRJ2	1.0531	0.831	1.C589	C.845	1.C649	C.819	1.C709	C.863

Table 3c Ganymede/ Sun

J3B	0.3341	0.384	0.3346	0.385	0.3353	0.271	0.3355	0.445
J3B	0.3362	0.559	0.3365	0.469	0.3369	0.645	0.3374	0.533
J3B	0.3379	0.663	0.3384	0.898	0.3389	0.613	0.3394	0.625
J3C	0.3399	0.722	0.3404	0.516	0.3409	0.504	0.3414	0.650
J3F	0.3419	0.603	0.3424	0.797	0.3429	0.562	0.3434	0.671
J3B	0.3440	0.633	0.3445	0.735	0.345	0.602	0.3455	0.546
J3B	0.3461	0.693	0.3466	0.847	0.3471	0.762	0.3477	0.724
J3B	0.3482	0.663	0.3487	0.727	0.3493	0.716	0.3498	0.659
J3B	0.3514	0.582	0.3519	0.675	0.3515	0.727	0.3521	0.697
J3B	0.3526	0.736	0.3532	0.632	0.3538	0.664	0.3544	0.679
J3B	0.3549	0.669	0.3555	0.664	0.3561	0.589	0.3567	0.570
J3B	0.3573	0.581	0.3579	0.554	0.3585	0.613	0.3591	0.528
J3B	0.3597	0.553	0.3603	0.523	0.3609	0.660	0.3615	0.581
J3B	0.3621	0.577	0.3628	0.578	0.3634	0.569	0.3641	0.573
J3B	0.3647	0.602	0.3653	0.645	0.3659	0.640	0.3666	0.670
J3B	0.3672	0.603	0.3679	0.608	0.3685	0.653	0.3692	0.708
J3B	0.3699	0.641	0.3705	0.642	0.3712	0.655	0.3719	0.706
J3B	0.3726	0.684	0.3733	0.714	0.3741	0.726	0.3746	0.704
J3B	0.3753	0.726	0.3760	0.723	0.3767	0.736	0.3775	0.766
J3B	0.3782	0.743	0.3789	0.715	0.3796	0.764	0.3804	0.764
J3B	0.3811	0.778	0.3818	0.776	0.3826	0.787	0.3833	0.797
J3B	0.3841	0.807	0.3848	0.830	0.3856	0.817	0.3864	0.800
J3B	0.3871	0.797	0.3879	0.782	0.3887	0.797	0.3895	0.774
J3B	0.3903	0.784	0.3911	0.765	0.3919	0.766	0.3927	0.782
J3B	0.3935	0.794	0.3943	0.779	0.3952	0.785	0.3960	0.792
J3B	0.3968	0.769	0.3977	0.777	0.3985	0.774	0.3994	0.791
J3B	0.4002	0.782	0.4011	0.775	0.4020	0.816	0.4029	0.839
J3B	0.4037	0.85	0.4046	0.851	0.4055	0.846	0.4064	0.854
J3B	0.4073	0.837	0.4083	0.835	0.4092	0.833	0.4101	0.837
J3B	0.4110	0.840	0.4120	0.859	0.4129	0.852	0.4139	0.851
J3B	0.4149	0.866	0.4158	0.843	0.4168	0.877	0.4178	0.873
J3B	0.4188	0.868	0.4198	0.862	0.4208	0.853	0.4218	0.868
J3B	0.4228	0.859	0.4239	0.864	0.4249	0.868	0.4259	0.863
J3B	0.4271	0.856	0.4281	0.859	0.4291	0.852	0.4302	0.856
J3B	0.4313	0.863	0.4324	0.854	0.4335	0.859	0.4346	0.856
J3B	0.4357	0.872	0.4368	0.863	0.4381	0.878	0.4391	0.882
J3B	0.4403	0.884	0.4414	0.886	0.4425	0.896	0.4438	0.891
J3B	0.4451	0.895	0.4462	0.892	0.4474	0.895	0.4486	0.905
J3B	0.4499	0.919	0.4511	0.902	0.4524	0.907	0.4536	0.901
J3B	0.4549	0.902	0.4562	0.903	0.4575	0.904	0.4588	0.907
J3B	0.4601	0.915	0.4614	0.917	0.4628	0.922	0.4641	0.918
J3B	0.4655	0.927	0.4669	0.929	0.4683	0.934	0.4697	0.933
J3B	0.4711	0.934	0.4725	0.926	0.4739	0.944	0.4754	0.947
J3B	0.4769	0.959	0.4783	0.957	0.4798	0.966	0.4813	0.966
J3B	0.4829	0.972	0.4844	0.973	0.4859	0.973	0.4875	0.976
J3B	0.4891	0.973	0.4907	0.969	0.4923	0.975	0.4939	0.977
J3B	0.4955	0.972	0.4972	0.959	0.4986	0.950	0.5005	0.952

Table 3c cont. Ganymede/ Sun

J3B		0.5022	0.946	0.5039	0.955	0.5057	0.955	0.5074	0.951
J3B		0.5092	0.963	0.5110	0.968	0.5128	0.965	0.5146	0.972
J3B		0.5164	0.968	0.5183	0.975	0.5201	0.984	0.5220	0.983
J3B		0.5239	0.991	0.5259	0.984	0.5278	0.989	0.5298	0.988
J3B		0.5313	0.991	0.5338	0.989	0.5359	0.998	0.5379	0.997
J3B		0.5400	0.994	0.5421	1.001	0.5442	1.002	0.5464	1.003
	IRJ3	0.5490	0.879	0.5499	0.907	0.5508	0.946	0.5517	0.959
	IRJ3	0.5526	0.969	0.5535	0.984	0.5544	0.996	0.5553	1.003
	IRJ3	0.5563	0.996	0.5572	1.006	0.5582	0.998	0.5591	1.006
	IRJ3	0.5601	1.006	0.5610	0.995	0.5620	0.997	0.5630	1.009
	IRJ3	0.5639	1.012	0.5649	1.005	0.5659	1.014	0.5669	1.011
	IRJ3	0.5679	1.017	0.5689	1.014	0.5699	1.018	0.5709	1.012
	IRJ3	0.5720	1.015	0.5730	1.016	0.5740	1.020	0.5751	1.019
	IRJ3	0.5761	1.022	0.5772	1.020	0.5782	1.022	0.5793	1.025
	IRJ3	0.5804	1.024	0.5814	1.033	0.5825	1.030	0.5836	1.028
	IRJ3	0.5847	1.040	0.5858	1.041	0.5869	1.032	0.5881	1.037
	IRJ3	0.5892	1.029	0.5903	1.029	0.5915	1.032	0.5926	1.041
	IRJ3	0.5938	1.033	0.5949	1.044	0.5961	1.045	0.5973	1.046
	IRJ3	0.5984	1.053	0.5996	1.052	0.6008	1.045	0.6020	1.057
	IRJ3	0.6033	1.050	0.6045	1.053	0.6057	1.058	0.6069	1.059
	IRJ3	0.6082	1.062	0.6094	1.053	0.6107	1.057	0.6120	1.064
	IRJ3	0.6133	1.061	0.6145	1.065	0.6158	1.056	0.6171	1.063
	IRJ3	0.6185	1.063	0.6198	1.061	0.6211	1.067	0.6224	1.063
	IRJ3	0.6238	1.066	0.6252	1.068	0.6265	1.074	0.6279	1.069
	IRJ3	0.6293	1.069	0.6307	1.069	0.6321	1.078	0.6335	1.074
	IRJ3	0.6349	1.075	0.6364	1.072	0.6378	1.072	0.6393	1.081
	IRJ3	0.6407	1.074	0.6422	1.080	0.6437	1.081	0.6452	1.085
	IRJ3	0.6467	1.085	0.6482	1.084	0.6497	1.085	0.6513	1.091
	IRJ3	0.6528	1.085	0.6544	1.089	0.6560	1.093	0.6575	1.097
	IRJ3	0.6591	1.094	0.6607	1.097	0.6624	1.088	0.6640	1.090
	IRJ3	0.6656	1.088	0.6673	1.083	0.6690	1.091	0.6707	1.084
	IRJ3	0.6723	1.081	0.6741	1.092	0.6758	1.096	0.6775	1.094
	IRJ3	0.6793	1.096	0.6810	1.095	0.6828	1.101	0.6846	1.098
	IRJ3	0.6864	1.101	0.6882	1.105	0.6900	1.105	0.6919	1.104
	IRJ3	0.6937	1.103	0.6956	1.100	0.6975	1.101	0.6994	1.097
	IRJ3	0.7013	1.098	0.7033	1.101	0.7052	1.100	0.7072	1.099
	IRJ3	0.7092	1.093	0.7112	1.094	0.7132	1.093	0.7152	1.086
	IRJ3	0.7173	1.085	0.7193	1.089	0.7214	1.084	0.7235	1.085
	IRJ3	0.7256	1.085	0.7278	1.082	0.7299	1.082	0.7321	1.079
	IRJ3	0.7343	1.074	0.7365	1.068	0.7387	1.079	0.7410	1.076
	IRJ3	0.7432	1.081	0.7455	1.084	0.7478	1.093	0.7502	1.079
	IRJ3	0.7525	1.085	0.7549	1.082	0.7573	1.074	0.7597	1.072
	IRJ3	0.7622	1.087	0.7646	1.081	0.7671	1.077	0.7696	1.074
	IRJ3	0.7721	1.069	0.7747	1.072	0.7773	1.071	0.7799	1.065
	IRJ3	0.7825	1.071	0.7851	1.067	0.7878	1.056	0.7905	1.061
	IRJ3	0.7932	1.057	0.7960	1.058	0.7988	1.049	0.8016	1.047
	IRJ3	0.8044	1.055	0.8073	1.052	0.8102	1.058	0.8131	1.057
	IRJ3	0.8160	1.068	0.8190	1.071	0.8220	1.087	0.8250	1.088

Table 3c cont. Ganymede/ Sun

IRJ3	0.8281	1.093	0.8312	1.091	0.8344	1.093	0.8375	1.088
IRJ3	0.8407	1.098	0.8439	1.109	0.8472	1.109	0.8505	1.125
IRJ3	0.8538	1.128	0.8572	1.131	0.8606	1.126	0.8641	1.133
IRJ3	0.8675	1.138	0.8711	1.156	0.8746	1.172	0.8782	1.186
IRJ3	0.8819	1.190	0.8855	1.195	0.8893	1.189	0.8930	1.183
IRJ3	0.8968	1.181	0.9007	1.167	0.9046	1.160	0.9085	1.136
IRJ3	0.9125	1.127	0.9165	1.111	0.9206	1.100	0.9247	1.071
IRJ3	0.9289	1.059	0.9331	1.044	0.9374	1.047	0.9417	1.041
IRJ3	0.9461	1.042	0.9505	1.021	0.9550	1.009	0.9595	1.007
IRJ3	0.9641	0.995	0.9688	0.998	0.9735	0.980	0.9783	0.958
IRJ3	0.9831	0.959	0.9880	0.949	0.9930	0.942	0.9980	0.924
IRJ3	1.0031	0.920	1.0083	0.909	1.0135	0.895	1.0188	0.884
IRJ3	1.0242	0.864	1.0296	0.880	1.0351	0.863	1.0407	0.874
IRJ3	1.0464	0.864	1.0521	0.874	1.0580	0.888	1.0639	0.934

Table 3d Callisto/ Sun

J4B	0.3341	0.158	0.3346	0.311	0.3350	0.269	0.3355	0.219
J4B	0.3360	0.361	0.3365	0.271	0.3369	0.130	0.3374	0.309
J4B	0.3379	0.325	0.3384	0.358	0.3389	0.368	0.3394	0.284
J4B	0.3399	0.408	0.3404	0.306	0.3409	0.201	0.3414	0.292
J4B	0.3419	0.380	0.3424	0.412	0.3429	0.339	0.3434	0.208
J4B	0.3440	0.221	0.3445	0.285	0.3450	0.383	0.3455	0.346
J4B	0.3461	0.357	0.3466	0.376	0.3471	0.376	0.3477	0.328
J4B	0.3482	0.374	0.3487	0.405	0.3493	0.436	0.3498	0.349
J4B	0.3504	0.400	0.3510	0.391	0.3515	0.358	0.3521	0.377
J4B	0.3526	0.386	0.3532	0.379	0.3538	0.329	0.3544	0.350
J4B	0.3549	0.393	0.3555	0.389	0.3561	0.386	0.3567	0.382
J4B	0.3573	0.379	0.3579	0.376	0.3585	0.403	0.3591	0.365
J4B	0.3597	0.388	0.3603	0.393	0.3609	0.317	0.3615	0.336
J4B	0.3621	0.325	0.3628	0.325	0.3634	0.350	0.3640	0.350
J4B	0.3647	0.369	0.3653	0.386	0.3659	0.383	0.3666	0.425
J4B	0.3672	0.462	0.3679	0.471	0.3685	0.489	0.3692	0.427
J4B	0.3699	0.452	0.3705	0.481	0.3712	0.452	0.3719	0.456
J4B	0.3726	0.448	0.3733	0.438	0.3740	0.445	0.3746	0.479
J4B	0.3753	0.499	0.3760	0.512	0.3768	0.547	0.3775	0.559
J4B	0.3782	0.562	0.3789	0.572	0.3796	0.578	0.3804	0.604
J4B	0.3811	0.600	0.3818	0.616	0.3826	0.608	0.3833	0.619
J4B	0.3841	0.606	0.3848	0.616	0.3856	0.619	0.3864	0.613
J4B	0.3871	0.618	0.3879	0.616	0.3887	0.600	0.3895	0.600
J4B	0.3903	0.618	0.3911	0.599	0.3919	0.608	0.3927	0.599
J4B	0.3935	0.592	0.3943	0.598	0.3952	0.592	0.3960	0.608
J4B	0.3968	0.600	0.3977	0.615	0.3985	0.609	0.3994	0.616
J4B	0.4002	0.623	0.4011	0.616	0.4020	0.608	0.4029	0.615
J4B	0.4037	0.606	0.4046	0.610	0.4055	0.623	0.4064	0.631
J4B	0.4073	0.632	0.4083	0.630	0.4092	0.631	0.4101	0.628
J4B	0.4110	0.626	0.4120	0.636	0.4129	0.645	0.4139	0.658
J4B	0.4149	0.651	0.4158	0.651	0.4168	0.657	0.4178	0.670
J4B	0.4188	0.666	0.4198	0.674	0.4208	0.682	0.4218	0.678
J4B	0.4228	0.673	0.4239	0.671	0.4249	0.676	0.4259	0.674
J4B	0.4270	0.669	0.4281	0.672	0.4291	0.676	0.4302	0.677
J4B	0.4313	0.682	0.4324	0.675	0.4335	0.687	0.4346	0.678
J4B	0.4357	0.675	0.4368	0.678	0.4380	0.682	0.4391	0.687
J4B	0.4403	0.691	0.4414	0.699	0.4426	0.702	0.4438	0.705
J4B	0.4450	0.712	0.4462	0.722	0.4474	0.728	0.4486	0.730
J4B	0.4499	0.719	0.4511	0.707	0.4524	0.706	0.4536	0.708
J4B	0.4549	0.708	0.4562	0.715	0.4575	0.718	0.4588	0.726
J4B	0.4601	0.728	0.4614	0.732	0.4628	0.730	0.4641	0.725
J4B	0.4655	0.740	0.4669	0.740	0.4683	0.748	0.4697	0.765
J4B	0.4711	0.776	0.4725	0.769	0.4739	0.768	0.4754	0.766
J4B	0.4769	0.770	0.4783	0.773	0.4798	0.777	0.4813	0.783
J4B	0.4829	0.781	0.4844	0.779	0.4859	0.787	0.4875	0.785
J4B	0.4891	0.787	0.4907	0.788	0.4923	0.786	0.4939	0.785
J4B	0.4955	0.782	0.4972	0.766	0.4988	0.748	0.5005	0.734
J4B	0.5022	0.737	0.5039	0.737	0.5057	0.742	0.5074	0.740

Table 3d cont. Callisto/ Sun

J4B	0.5092	0.738	0.5110	0.742	0.5128	0.748	0.5146	0.746
J4B	0.5164	0.750	0.5183	0.752	0.5201	0.754	0.5220	0.757
J4B	0.5239	0.759	0.5259	0.760	0.5278	0.767	0.5298	0.768
J4B	0.5318	0.770	0.5338	0.772	0.5359	0.772	0.5379	0.771
J4B	0.5400	0.774	0.5421	0.774	0.5442	0.778	0.5464	0.781
IRJ4	0.5499	0.951	0.5509	0.976	0.5518	0.990	0.5527	0.996
IRJ4	0.5536	1.007	0.5545	0.998	0.5555	1.002	0.5564	1.006
IRJ4	0.5573	1.003	0.5583	1.006	0.5592	1.010	0.5602	1.007
IRJ4	0.5612	1.020	0.5621	1.010	0.5631	1.013	0.5641	1.013
IRJ4	0.5651	1.019	0.5661	1.015	0.5671	1.021	0.5681	1.027
IRJ4	0.5691	1.017	0.5701	1.021	0.5711	1.021	0.5721	1.016
IRJ4	0.5732	1.026	0.5742	1.024	0.5753	1.027	0.5763	1.022
IRJ4	0.5774	1.029	0.5784	1.031	0.5795	1.029	0.5806	1.040
IRJ4	0.5817	1.030	0.5828	1.030	0.5839	1.033	0.5850	1.034
IRJ4	0.5861	1.027	0.5872	1.025	0.5883	1.035	0.5895	1.037
IRJ4	0.5906	1.035	0.5917	1.035	0.5929	1.041	0.5941	1.052
IRJ4	0.5952	1.040	0.5964	1.043	0.5976	1.044	0.5988	1.045
IRJ4	0.6000	1.048	0.6012	1.045	0.6024	1.046	0.6036	1.051
IRJ4	0.6048	1.054	0.6061	1.053	0.6073	1.050	0.6086	1.051
IRJ4	0.6098	1.045	0.6111	1.049	0.6124	1.045	0.6137	1.051
IRJ4	0.6150	1.057	0.6163	1.056	0.6176	1.061	0.6189	1.065
IRJ4	0.6202	1.058	0.6216	1.052	0.6229	1.055	0.6243	1.056
IRJ4	0.6256	1.063	0.6270	1.060	0.6284	1.063	0.6298	1.063
IRJ4	0.6312	1.063	0.6326	1.065	0.6340	1.058	0.6355	1.064
IRJ4	0.6369	1.061	0.6384	1.066	0.6398	1.065	0.6413	1.067
IRJ4	0.6428	1.072	0.6443	1.070	0.6458	1.065	0.6473	1.068
IRJ4	0.6488	1.074	0.6504	1.069	0.6519	1.067	0.6535	1.079
IRJ4	0.6551	1.084	0.6567	1.082	0.6583	1.077	0.6599	1.082
IRJ4	0.6615	1.070	0.6631	1.072	0.6648	1.068	0.6664	1.075
IRJ4	0.6681	1.069	0.6698	1.069	0.6715	1.071	0.6732	1.070
IRJ4	0.6749	1.075	0.6766	1.075	0.6784	1.079	0.6801	1.073
IRJ4	0.6819	1.077	0.6837	1.079	0.6855	1.078	0.6873	1.089
IRJ4	0.6891	1.088	0.6910	1.083	0.6928	1.084	0.6947	1.081
IRJ4	0.6966	1.084	0.6985	1.090	0.7004	1.080	0.7024	1.077
IRJ4	0.7043	1.085	0.7063	1.076	0.7083	1.080	0.7103	1.080
IRJ4	0.7123	1.066	0.7143	1.065	0.7164	1.072	0.7184	1.075
IRJ4	0.7205	1.066	0.7226	1.068	0.7247	1.068	0.7269	1.066
IRJ4	0.7290	1.065	0.7312	1.068	0.7334	1.068	0.7356	1.073
IRJ4	0.7378	1.073	0.7401	1.072	0.7424	1.075	0.7447	1.072
IRJ4	0.7470	1.076	0.7493	1.074	0.7517	1.073	0.7540	1.073
IRJ4	0.7564	1.076	0.7588	1.094	0.7613	1.102	0.7637	1.087
IRJ4	0.7662	1.078	0.7687	1.079	0.7713	1.069	0.7738	1.078
IRJ4	0.7764	1.076	0.7790	1.085	0.7816	1.082	0.7843	1.080
IRJ4	0.7870	1.073	0.7897	1.065	0.7924	1.068	0.7951	1.055
IRJ4	0.7979	1.066	0.8007	1.059	0.8036	1.061	0.8064	1.067
IRJ4	0.8093	1.066	0.8122	1.066	0.8152	1.070	0.8182	1.080
IRJ4	0.8212	1.076	0.8242	1.080	0.8273	1.090	0.8304	1.080
IRJ4	0.8335	1.091	0.8367	1.084	0.8399	1.088	0.8431	1.092
IRJ4	0.8464	1.075	0.8497	1.078	0.8531	1.074	0.8564	1.084

Table 3d Callisto/ Sun

IRJ4	0.8598	1.083	0.8633	1.093	0.8668	1.094	0.8703	1.101
IRJ4	0.8739	1.107	0.8775	1.110	0.8811	1.129	0.8848	1.119
IRJ4	0.8885	1.117	0.8923	1.106	0.8961	1.109	0.9000	1.119
IRJ4	0.9038	1.118	0.9078	1.117	0.9118	1.122	0.9158	1.109
IRJ4	0.9199	1.108	0.9240	1.101	0.9282	1.110	0.9324	1.128
IRJ4	0.9367	1.110	0.9411	1.112	0.9454	1.113	0.9499	1.115
IRJ4	0.9544	1.106	0.9589	1.090	0.9635	1.075	0.9682	1.086
IRJ4	0.9729	1.070	0.9777	1.044	0.9826	1.057	0.9875	1.014
IRJ4	0.9925	1.035	0.9975	1.027	1.0026	1.026	1.0078	1.019
IRJ4	1.0130	1.017	1.0183	1.040	1.0237	1.021	1.0292	0.989
IRJ4	1.0347	1.011	1.0403	1.044	1.0460	1.018	1.0518	1.018
IRJ4	1.0576	1.051	1.0636	1.065	1.0696	1.126	1.0757	1.215

Table 4

10 TAU/SUN BEST 12/76 VSS

LAMBDA	RATIO 1	AVG DEV	LAMBDA	RATIO 1	AVG DEV
0.3345	1.190626	0.058259	0.5675	1.000000	0.010478
0.3530	1.180346	0.066325	0.6040	1.000089	0.011366
0.3780	1.140174	0.050835	0.6310	0.991398	0.010881
0.4040	1.169151	0.043588	0.6680	0.985605	0.014286
0.4300	1.082713	0.045120	0.7010	0.982427	0.023987
0.4675	1.046880	0.015527	0.7340	0.961191	0.014949
0.5020	1.034966	0.011241	0.7645	0.964815	0.016655
0.5365	1.022382	0.010169	0.8000	0.953240	0.016796
0.8310	0.939220	0.018007	1.0990	0.881625	0.053960
0.8660	0.922296	0.018081			
0.8990	0.927020	0.020220			
0.9330	0.927352	0.021922			
0.9700	0.928200	0.020220			
1.0010	0.905073	0.022163			
1.0330	0.911445	0.023826			
1.0640	0.888690	0.025943			

Table 5 10 Tau/ Sun

0.3282	1.174	0.3286	1.176	0.3291	1.177	0.3295	1.178
0.3300	1.179	0.3304	1.180	0.3309	1.181	0.3313	1.182
0.3318	1.184	0.3322	1.185	0.3327	1.186	0.3332	1.187
0.3336	1.188	0.3341	1.190	0.3346	1.191	0.3350	1.190
0.3355	1.190	0.3360	1.190	0.3365	1.189	0.3370	1.189
0.3374	1.189	0.3379	1.189	0.3384	1.188	0.3389	1.188
0.3394	1.188	0.3399	1.188	0.3404	1.187	0.3409	1.187
0.3414	1.187	0.3419	1.186	0.3424	1.186	0.3429	1.186
0.3435	1.186	0.3440	1.185	0.3445	1.185	0.3450	1.185
0.3456	1.184	0.3461	1.184	0.3466	1.184	0.3472	1.184
0.3477	1.183	0.3482	1.183	0.3488	1.183	0.3493	1.182
0.3499	1.182	0.3504	1.182	0.3510	1.181	0.3516	1.181
0.3521	1.181	0.3527	1.180	0.3533	1.180	0.3538	1.179
0.3544	1.178	0.3550	1.177	0.3556	1.176	0.3562	1.175
0.3567	1.174	0.3573	1.173	0.3579	1.172	0.3585	1.171
0.3591	1.170	0.3597	1.169	0.3604	1.168	0.3610	1.167
0.3616	1.166	0.3622	1.165	0.3628	1.164	0.3635	1.163
0.3641	1.162	0.3647	1.161	0.3654	1.160	0.3660	1.159
0.3667	1.158	0.3673	1.157	0.3680	1.156	0.3686	1.155
0.3693	1.154	0.3699	1.153	0.3706	1.152	0.3713	1.151
0.3720	1.150	0.3727	1.149	0.3733	1.148	0.3740	1.146
0.3747	1.145	0.3754	1.144	0.3761	1.143	0.3768	1.142
0.3776	1.141	0.3783	1.140	0.3790	1.141	0.3797	1.142
0.3805	1.143	0.3812	1.144	0.3819	1..144	0.3827	1.145
0.3834	1.146	0.3842	1.147	0.3849	1.148	0.3857	1.149
0.3865	1.150	0.3873	1.150	0.3880	1.151	0.3888	1.152
0.3896	1.153	0.3904	1.154	0.3912	1.155	0.3920	1.156
0.3928	1.157	0.3936	1.158	0.3945	1.158	0.3953	1.159
0.3961	1.160	0.3970	1.161	0.3978	1.162	0.3987	1.163
0.3995	1.164	0.4004	1.165	0.4012	1.166	0.4021	1.167
0.4030	1.168	0.4039	1.169	0.4048	1.167	0.4057	1.164
0.4066	1.161	0.4075	1.157	0.4084	1.154	0.4093	1.151
0.4103	1.148	0.4112	1.145	0.4122	1.142	0.4131	1.139
0.4141	1.136	0.4150	1.132	0.4160	1.129	0.4170	1.126
0.4180	1.123	0.4190	1.119	0.4200	1.116	0.4210	1.113
0.4220	1.109	0.4230	1.105	0.4241	1.102	0.4251	1.099
0.4261	1.096	0.4272	1.092	0.4283	1.088	0.4293	1.085
0.4304	1.082	0.4315	1.081	0.4326	1.080	0.4337	1.079
0.4348	1.078	0.4359	1.077	0.4371	1.076	0.4382	1.075
0.4394	1.074	0.4405	1.073	0.4417	1.072	0.4429	1.070
0.4441	1.069	0.4453	1.068	0.4465	1.067	0.4477	1.066
0.4489	1.065	0.4501	1.063	0.4514	1.062	0.4527	1.061
0.4539	1.060	0.4552	1.059	0.4565	1.057	0.4578	1.056
0.4591	1.055	0.4604	1.054	0.4618	1.052	0.4631	1.051
0.4645	1.050	0.4658	1.048	0.4672	1.047	0.4686	1.046
0.4700	1.046	0.4714	1.045	0.4729	1.045	0.4743	1.044

Table 5 cont. 10 Tau/ Sun

0.4758	1.044	0.4772	1.043	0.4787	1.043	0.4802	1.042
0.4817	1.042	0.4832	1.041	0.4848	1.041	0.4863	1.040
0.4879	1.040	0.4895	1.039	0.4911	1.039	0.4927	1.038
0.4943	1.038	0.4959	1.037	0.4976	1.036	0.4993	1.036
0.5010	1.035	0.5027	1.035	0.5044	1.034	0.5061	1.033
0.5079	1.033	0.5097	1.032	0.5114	1.031	0.5132	1.031
0.5151	1.030	0.5169	1.029	0.5188	1.029	0.5207	1.028
0.5226	1.027	0.5245	1.027	0.5264	1.026	0.5284	1.025
0.5304	1.025	0.5324	1.024	0.5344	1.023	0.5364	1.022
0.5385	1.021	0.5406	1.019	0.5427	1.018	0.5448	1.016
0.5470	1.015	0.5492	1.013	0.5514	1.012	0.5536	1.010
0.5559	1.008	0.5582	1.007	0.5605	1.005	0.5628	1.003
0.5652	1.002	0.5675	1.000	0.5700	0.998	0.5724	0.996
0.5749	0.995	0.5774	0.993	0.5799	0.991	0.5824	0.989
0.5850	0.987	0.5877	0.985	0.5903	0.984	0.5930	0.982
0.5957	0.980	0.5985	0.978	0.6012	0.976	0.6041	0.974
0.6069	0.972	0.6098	0.970	0.6127	0.967	0.6157	0.965
0.6187	0.963	0.6217	0.961	0.6248	0.959	0.6279	0.957

T

0.5353	1.023	0.5361	1.022	0.5369	1.022	0.5378	1.021
0.5386	1.021	0.5395	1.020	0.5403	1.020	0.5412	1.019
0.5420	1.018	0.5429	1.018	0.5438	1.017	0.5446	1.016
0.5455	1.016	0.5464	1.015	0.5473	1.015	0.5482	1.014
0.5491	1.013	0.5500	1.013	0.5509	1.012	0.5518	1.011
0.5527	1.011	0.5536	1.010	0.5546	1.009	0.5555	1.009
0.5564	1.008	0.5574	1.007	0.5583	1.007	0.5593	1.006
0.5602	1.005	0.5612	1.005	0.5622	1.004	0.5632	1.003
0.5641	1.002	0.5651	1.002	0.5661	1.001	0.5671	1.000
0.5681	1.000	0.5691	1.000	0.5702	1.000	0.5712	1.000
0.5722	1.000	0.5732	1.000	0.5743	1.000	0.5753	1.000
0.5764	1.000	0.5774	1.000	0.5785	1.000	0.5796	1.000
0.5807	1.000	0.5817	1.000	0.5828	1.000	0.5839	1.000
0.5850	1.000	0.5862	1.000	0.5873	1.000	0.5884	1.000
0.5895	1.000	0.5907	1.000	0.5918	1.000	0.5930	1.000
0.5941	1.000	0.5953	1.000	0.5965	1.000	0.5977	1.000
0.5989	1.000	0.6001	1.000	0.6013	1.000	0.6025	1.000
0.6037	1.000	0.6049	1.000	0.6062	0.999	0.6074	0.999
0.6087	0.998	0.6099	0.998	0.6112	0.998	0.6125	0.997
0.6138	0.997	0.6151	0.996	0.6164	0.996	0.6177	0.996
0.6190	0.995	0.6204	0.995	0.6217	0.994	0.6230	0.994
0.6244	0.993	0.6258	0.993	0.6272	0.993	0.6285	0.992
0.6299	0.992	0.6313	0.991	0.6328	0.991	0.6342	0.991
0.6356	0.991	0.6371	0.990	0.6385	0.990	0.6400	0.990
0.6415	0.990	0.6430	0.989	0.6445	0.989	0.6460	0.989
0.6475	0.989	0.6490	0.989	0.6506	0.988	0.6521	0.988
0.6537	0.988	0.6552	0.988	0.6568	0.987	0.6584	0.987

Table 5 cont. 10 Tau/ Sun

0.6600	0.987	0.6617	0.987	0.6633	0.986	0.6649	0.986
0.6666	0.986	0.6683	0.986	0.6700	0.985	0.6717	0.985
0.6734	0.985	0.6751	0.985	0.6768	0.985	0.6786	0.985
0.6803	0.984	0.6821	0.984	0.6839	0.984	0.6857	0.984
0.6875	0.984	0.6894	0.984	0.6912	0.983	0.6931	0.983
0.6950	0.983	0.6969	0.983	0.6988	0.983	0.7007	0.982
0.7026	0.981	0.7046	0.980	0.7065	0.979	0.7085	0.978
0.7105	0.976	0.7126	0.975	0.7146	0.974	0.7166	0.972
0.7187	0.971	0.7208	0.970	0.7229	0.968	0.7250	0.967
0.7272	0.966	0.7293	0.964	0.7315	0.963	0.7337	0.961
0.7359	0.961	0.7382	0.962	0.7404	0.962	0.7427	0.962
0.7450	0.962	0.7473	0.963	0.7497	0.963	0.7520	0.963
0.7544	0.964	0.7568	0.964	0.7592	0.964	0.7617	0.964
0.7641	0.965	0.7666	0.964	0.7691	0.963	0.7717	0.962
0.7742	0.962	0.7768	0.961	0.7794	0.960	0.7821	0.959
0.7847	0.958	0.7874	0.957	0.7901	0.956	0.7928	0.956
0.7956	0.955	0.7984	0.954	0.8012	0.953	0.8040	0.951
0.8069	0.950	0.8098	0.949	0.8127	0.947	0.8157	0.946
0.8187	0.945	0.8217	0.943	0.8248	0.942	0.8278	0.941
0.8310	0.939	0.8341	0.938	0.8373	0.936	0.8405	0.935
0.8437	0.933	0.8470	0.931	0.8503	0.930	0.8537	0.928
0.8571	0.927	0.8605	0.925	0.8639	0.923	0.8674	0.922
0.8710	0.923	0.8745	0.923	0.8782	0.924	0.8818	0.924
0.8855	0.925	0.8892	0.926	0.8930	0.926	0.8968	0.927
0.9007	0.927	0.9046	0.927	0.9086	0.927	0.9126	0.927
0.9166	0.927	0.9207	0.927	0.9249	0.927	0.9290	0.927
0.9333	0.927	0.9376	0.927	0.9419	0.928	0.9463	0.928
0.9508	0.928	0.9553	0.928	0.9599	0.928	0.9645	0.928
0.9692	0.928	0.9739	0.925	0.9787	0.922	0.9836	0.918
0.9885	0.914	0.9935	0.911	0.9986	0.907	1.0037	0.906
1.0089	0.907	1.0141	0.908	1.0195	0.909	1.0249	0.910
1.0304	0.911	1.0359	0.909	1.0416	0.905	1.0473	0.901
1.0531	0.897	1.0589	0.892	1.0649	0.888	1.0709	0.887
1.0771	0.886	1.0833	0.885	1.0896	0.883	1.0960	0.882

BIBLIOGRAPHY & REFERENCES

Bergstrahl, J.T., Matson, D.L., Johnson, T.V.,"Sodium D-line emission from Io: synoptic observations from Table Mountain Observatory", Ap.J.,195,L1-L5,(1975).

Binder, A.B. and Cruikshank, D.P.,"Evidence for an atmosphere on Io", Icarus, 3,299-305, (1964).

Binder, A.B. and Cruikshank, D.P., "Photometric search for atmospheres on Europa and Ganymede", Icarus, 5, 7-9, (1966).

Blanco, C. and Catalano, S.,"On the photometric variations of the Saturn and Jupiter satellites", Astron. Astrophys.,33,105-111, (1974).

Caldwell, J.,"UV observations of small bodies in the Solar System by OAO-2", Icarus, 25, 384-396, (1975).

Dollfus, A.,"Optical polarimetry of the Galilean satellites of Jupiter", Icarus, 25, 416-431, (1975).

Elias, J.,"Standard Star Calibrations for Planetary Observations", M.S. Thesis, Mass. Inst. Tech., (1972).

Fallon, F.W. and Murphy, R.E.,"Absence of post-eclipse brightening of Io and Europa in 1970", Icarus, 14, (1971).

Fanale, F.P., Johnson, T.V., Matson, D.L.,"Io: a surface evaporite deposit", Science, 186, 922-925, (1974).

Fink, U. and Burk, S.D.,"Reflection spectra, 2.5-7 μm, of some solids of planetary interest", Comm. Lunar Planet. Sci. Lab, 10, no. 185, (1971).

Fink, U., Dekkers, N.H., Larson, H.P.,"Infrared spectra of the Galilean satellites of Jupiter", Ap.J., 179, L155-L159, (1973).

Fink, U., Larson, H.P., Howell, R., Rieke, G.H.,"Infrared spectra of Io and Titan and narrow band photometer measurements of the Galilean satellites", B.A.A.S., 7,386, (1975).

Fink, U., Larson, H.P., Gautier, T.N.,"New upper limits for atmospheric constituents on Io", Icarus, 27, 439-446, (1976).

Franz, O.G. and Millis, R.L.,"A search for an anomalous brightening of Io after eclipse", Icarus, 14, 13-15, (1970).

Gillett, F.C., Merrill, K.M., Stein, W.A.,"Albedo and thermal emission of Jovian satellites I-IV", Ap. Lett., 6, 247-249,(1970).

Gradie, J.,"A polarimetric survey of the Galilean satellites", B.A.A.S., 5, 404, (1974).

Greene, T.F., Vermillion, J.R., Shorthill, R.W., Clark, R.N., "The spectral reflectivity of select areas on Europa", Icarus, 25, 405-415, (1975).

Hansen, O.L.,"Infrared albedos and rotation curves of the Galilean satellites of Jupiter", Icarus, 26, 24-29, (1975).

Harris, D.L.,"Photmetry and colorimetry of planets and satellites", in Planets & Satellites, G.P. Kuiper and B.M. Middlehurst, eds., Univ. of Chicago Press, p.272, (1961).

Hayes,D.H.,"An absolute spectrophotometric calibration ...", Ap.J.,159,165-176, (1970)

Irvine, W.M., Pollack, J.B.,"Infrared optical properties of water and ice spheres", Icarus, 8, 324-360, (1968).

Johnson, T.V.,"Galilean satellites: narrowband photometry .30-1.10 m", Icarus, 14, 94-111, (1971).

Johnson, T.V.,"Albedo and spectral reflectivity of the Galilean satellites of Jupiter",PhD. Thesis, Calif. Inst. Tech.(1970).

Johnson, T.V., and McCord, T.B.,"Galilean satellites- spectral reflectivity .30-1.1 m", Icarus, 13, 37-42, (1970).

Johnson, T.V. and McCord, T.B.,"Spectral geometric albedo of the Galilean satellites, .3-2.5 m", Ap.J., 169, 589-594,(1971).

Johnson, T.V. and Pilcher, C.B.,"Satellite spectrophotometry and surface composition", in Planetary Satellites, J.A. Burns, ed. Univ. of Arizona Press, (1976).

Keegan, H.J. and Weidner, V.R.,"Infrared spectral reflectance of frost", J. Opt. Soc. Amer., 56, 523-524, (1966).

Keiffer, H.H.,"Spectral reflectance of CO_2-H_2O frosts",J. Geophys. Res., 75, 501, (1970).

Keiffer, H.H. and Smythe, W.D.,"Frost spectra comparison with Jupiter's satellites", Icarus, 21, 506-512, (1974).

Kuiper, G.P.,"Infrared Observations of planets and satellites", Astron. J., 62, 245, (1957).

Kuiper, G.P.,"Comments on the Galilean satellites", Comm. Lunar Planet. Sci. Lab, 10,28-33(1973).

Lebofsky, L.A. and Fegley, M.B.,"Laboratory reflection spectra for determination of chemical composition of icy bodies", Icarus, 28, 379-387, (1976).

Lee, T.,"Spectral albedo of the Galilean satellites", Comm. Lunar Planet. Sci. Lab,9, no. 168, (1971).

Lewis, J.S.,"Satellites of the outer planets: their physical and chemical nature", Icarus, 15, 174-185, (1971).

Lewis, J.S.,"Satellites of the outer planets: thermal models", Science, 172, 1127-1128, (1971).

Lewis, J.S.,"Low Temperature condensation from the solar nebula", Icarus, 16, 241-152, (1972).

Lewis, J.S.,"Metal/silicate fractionation in the solar system", Earth & Planet. Sci. Lett., 15, 286-290, (1972).

Lewis, J.S.,"Origin and composition of the terrestrial planets and satellites of the outer planets", in Origin of the Solar System, C.N.R.S., Paris, (1973).

Lewis, J.S.,"Chemistry of the outer Solar System", Space Sci. Rev., 14, 401-411, (1973).

Lewis, J.S.,"The chemistry of the Solar System", Sci. Am., 230, 51-65, (1974).

Matson, D.L., Johnson, T.V., Fanale, F.P.,"Sodium D-line emission from Io: sputtering and resonant scattering hypothesis", Ap.J., 192, L43, (1974).

McCord, T.B., Bosel, J., Frankston, M.J.,"Performance of the MIT silicon vidicon imaging system at the telescope", in Image Processing Techniques in Astronomy, de Jager/Nieuwenhuijzen, eds., D. Reidel Publishing Co. Dordrecht-Holland, 91-96, (1975).

McCord, T.B. and Frankston, M.J.,"Silicon diode array vidicons at the telescope: observational experience", App. Opt., 14, 1437-1446, (1975).

McFadden, L.A., McCord, T.B., Pieters, C.,"New visible spectral reflectance measurements of asteroid 4 Vesta", submitted to Icarus, (1977).

McElroy, M.B., Yung, Y.L., Brown, R.A.,"Sodium emission from Io: implications", Ap. J., 187, L127, (1974).

Millis, R.L. and Thompson, D.T.,"UBV photometry of the Galilean satellites", Icarus, 26, 408-419, (1975).

Moroz, V.I.,"Infrared spectrophotmetry of the Moon and Galilean satellites of Jupiter", Soviet Astron., 9, 999-1006, (1966).

Morrison, D., Morrison, N., Lazarewicz, A.R.,"Four-color photometry of the Galilean satellites", Icarus, 23, 399-416, (1974).

Morrison, D. and Cruikshank, D.L.,"Physical properties of the natural satellites", Space Sci. Rev., 15, 641-739, (1974).

Morrison, D. and Burns, J.A.,"The jovian satellites", in Jupiter, T. Gehrels, ed., U. of Ariz. Press, 991-1034, (1976).

Nash, D.B. and Fanale, F.P.,"Io's surface: composition based on reflectance spectra of sulfur/salt mixtures and proton irradiation experiments", submitted to Icarus, (1976).

Nygard, S.,"Alfa Lyrae / Sun flux measurements for calibration of planetary surface observations", M.S. Thesis, Mass. Inst. Tech., (1975).

O'Leary, B.T. and Veverka, J.,"On the anomalous brightening of Io after eclipse", Icarus, 14, 265-268, (1971).

O'Leary, B.T. and Miner, E.,"Another possible post-eclipse brightening of Io", Icarus, 20, 18, (1973).

Owen, F.N. and Lazor, F.J.,"Surface color variations of the Galilean satellites", Icarus, 19, 30-33, (1973).

Owensby, P.D., Pieters,C., Gaffey, M.J., Nygard, S., McCord, T.B., manuscript in preparation, (1977).

Pilcher, C.B., Ridgeway, S., McCord, T.B.,"Galilean satellites: identification of water frost", Science, 178, 1087-1089, (1972).

Pilcher, C.B. and Cruikshank, D.P.,"Galilean satellites: surface properties from near-infrared reflectance measurements", B.A.A.S., 8, 10, (1976).

Plummer, W.T.,"Infrared reflectivity of frost and the Venus clouds", J. Geophys. Res., 74, 3331-3336, (1969).

Rasool, S.I.,"Preliminary results on the atmospheres of Io and Jupiter from Pioneer 10 S-band occultation experiment", Science, 183, 323-324, (1974).

Sill, G.T.,"Reflection spectra of solids of planetary interest", Comm. Lunar Planet. Sci. Lab, 10, 1, (1973).

Sinton, W.M.,"Does Io have an atmosphere?", Icarus, 20, 284, (1973).

Smith, B.A. and Smith, S.A.,"Upper limits for an atmosphere on Io", Icarus, 17, 218-222, (1972).

Smythe, W.D.,"Spectra of hydrate frosts: their application to the outer Solar System", Icarus, 24, 421-427, (1975).

Stebbins, J.,"Light variations of the satellites of Jupiter", Lick Obs. Bull., 13, 1-11, (1927).

Stebbins, J. and Jacobsen, T.S.,"Further photometric measures of Jupiter's satellites", Lick Obs. Bull., 13, 180-195, (1928).

Trafton, L.,"High resolution spectra of Io's sodium emission", Ap. J., 202, L107-L112, (1975).

Trafton, L. and Macy, W.,"An oscillating asymmetry to Io's sodium emission cloud", Ap. J., 202, L155-L158, (1975).

Veverka, J.,"Polarization measurements of the Galilean satellites of Jupiter", Icarus, 14, 355-359, (1971).

Wamsteker, W.,"Narrow-band photometry of the Galilean satellites", Comm. Lunar Planet. Sci. Lab, 9, 171-177, (1972).

Wamsteker, W.,"A spectrophotometric study of the major planets and their large satellites", Univ. Ariz., PhD. thesis, (1975).

Wamsteker, W., Kroes, R.L., Fountain, J.A.,"On the surface compostion of Io", Icarus, 23, 417-424, (1974).